

Fast radio burst source properties and curvature radiation model

Pawan Kumar^{1*}, Wenbin Lu¹ and Mukul Bhattacharya²

¹*Department of Astronomy, University of Texas at Austin, Austin, TX 78712, USA*

²*Department of Physics, University of Texas at Austin, Austin, TX 78712, USA*

21 March 2017

ABSTRACT

We use the observed properties of fast radio bursts (FRBs) and a number of general physical considerations to provide a broad-brush model for the physical properties of FRB sources and the radiation mechanism. We show that the magnetic field in the source region should be at least 10^{14} Gauss. This strong field is required to ensure that the electrons have sufficiently high ground state Landau energy so that particle collisions, instabilities, and strong electromagnetic fields associated with the FRB radiation do not perturb electrons' motion in the direction transverse to the magnetic field and destroy their coherent motion; coherence is required by the high observed brightness temperature of FRB radiation. The electric field in the source region required to sustain particle motion for a wave period is estimated to be of order 10^{11} esu. These requirements suggest that FRBs are produced near the surface of magnetars perhaps via forced reconnection of magnetic fields to produce episodic, repeated, outbursts. The beaming-corrected energy release in these bursts is estimated to be about 10^{36} ergs, whereas the total energy in the magnetic field is at least $\sim 10^{45}$ ergs. We provide a number of predictions for this model which can be tested by future observations. One of which is that short duration FRB-like bursts should exist at much higher frequencies, possibly up to optical.

Key words: radiation mechanisms: coherent non-thermal - methods: analytical - radio: fast bursts, theory

1 INTRODUCTION

Fast radio bursts (FRBs) are Jansky-level millisecond duration transient events at \sim GHz frequencies of unknown physical origin discovered in pulsar surveys (Lorimer et al. 2007; Thornton et al. 2013). They have an all-sky rate of $\sim 10^3$ to 10^4 day⁻¹ above fluence ~ 1 Jy ms (Thornton et al. 2013; Keane & Petroff 2015; Rane et al. 2016; Champion et al. 2016). Very recently, the location of one of these bursts FRB 121102, a repeater, has been determined to an accuracy of $\sim 0.1''$ by interferometry with the Jansky Very Large Array (Spitler et al. 2016; Scholz et al. 2016; Chatterjee et al. 2017). This FRB is found to be associated with a dwarf star-forming host galaxy at redshift $z = 0.19273$ (Tendulkar et al. 2017). The FRB is also associated with a persistent radio source (Chatterjee et al. 2017), and their separation is further pinned down to $\lesssim 0.01''$ ($\lesssim 40$ pc in physical distance) by the European VLBI Network (Marcote et al. 2017).

It is not surprising that the distance of FRB 121102 is ~ 1 Gpc considering that many observational evidences had already suggested that FRBs are at cosmological distances (see Katz 2016a, for a brief review). First of all, their dispersion measures (the column density of free electrons along the line of sight $DM = \int n_e dl \sim 10^3$ pc cm⁻³) are much larger than the contribution from the in-

terstellar medium (ISM) in the Milky Way by roughly an order of magnitude¹. Second, if the DM is mostly contributed by an ionized nebula with electron temperature $T_e \sim 10^4$ K, then in order to avoid free-free absorption of GHz waves the size of the nebula must be larger than ~ 0.01 pc (Luan & Goldreich 2014). Moreover, the strength of H α and UV continuum flux limits combined with the free-free absorption argument suggest that at least the ‘‘Lorimer burst’’ FRB 010724 is at a distance $d \gtrsim 1$ Mpc (Kulkarni et al. 2014).

Confirmation of the cosmological origin means that FRBs are very energetic events. If the FRB sources are isotropic (the effect of anisotropy will be included later on), then the energy release is

$$E_{\text{iso}} = (1.3 \times 10^{40} \text{ erg}) \frac{\mathcal{F}}{\text{Jy ms}} d_{28}^2 \Delta\nu_9, \quad (1)$$

where \mathcal{F} is the fluence, $d = 10^{28} d_{28}$ cm is the luminosity distance and $\Delta\nu = \Delta\nu_9$ GHz is the width of the FRB spectrum. If FRB radiation is incoherent, for burst duration $\delta t = \delta t_{-3}$ ms, the area of the emitting region in the transverse direction — for a source with sub-relativistic speed — is $A < \pi(c\delta t)^2$, so the brightness

* E-mail: pk@astro.as.utexas.edu, wenbinlu@astro.as.utexas.edu

¹ A list of all reported FRBs and their properties can be found at <http://www.astronomy.swin.edu.au/pulsar/frbcatalog/> (Petroff et al. 2016).

temperature is

$$T_B = \frac{S_\nu d_A^2 c^2}{2A\nu^2 k_B} > (1 \times 10^{36} \text{ K}) \frac{S_\nu}{\text{Jy}} d_{A,28}^2 \delta t_{-3}^{-2} \nu_9^{-2}, \quad (2)$$

where S_ν is the peak specific flux, d_A is the angular diameter distance ($d_{A,28} \equiv d_A/10^{28} \text{ cm}$), $\nu = \nu_9 \text{ GHz}$ is the lab-frame frequency, c is speed of light, and k_B is the Boltzmann constant; we use the convenient notation $X_n \equiv X/10^n$ throughout the paper. Note that if the source is moving toward the Earth at Lorentz factor γ , then T'_B (the comoving frame temperature) is smaller by a factor of γ^3 than estimated in equation (2). For any reasonable Lorentz factor, the brightness temperature exceeds the Compton catastrophe limit of $T'_B \sim 10^{12} \text{ K}$. This means that FRB radiation must be coherent and the emitting particles relativistic, as pointed out by [Katz \(2014\)](#).

Regarding the nature of FRBs, the major unknowns are their progenitors and radiation mechanism. Many progenitor models have been proposed, including: collapsing neutron stars ([Falcke & Rezzolla 2014](#); [Zhang 2014](#)), neutron star or white dwarf mergers ([Piro 2012](#); [Kashiyama et al. 2013](#); [Totani 2013](#)), magnetar bursts² ([Popov & Postnov 2010](#); [Lyubarsky 2014](#); [Pen & Connor 2015](#); [Katz 2016b](#); [Murase et al. 2016](#)), supergiant pulses from young pulsars ([Connor et al. 2016](#); [Cordes & Wasserman 2016](#); [Katz 2016c](#); [Lyutikov et al. 2016](#); [Katz 2016d](#)), (Galactic) flaring stars ([Loeb et al. 2014](#)), relativistic jets running into clouds ([Romero et al. 2016](#)), asteroids colliding with neutron stars ([Geng & Huang 2015](#); [Dai et al. 2016](#)), close neutron star-white dwarf binaries ([Gu et al. 2016](#)), lightning in the neutron star magnetosphere ([Katz 2017](#)), and plasma stream sweeping across the neutron star magnetosphere ([Zhang 2017](#)). These works are only based on considerations of energetics and timescales, and the authors simply *assumed* that (a fraction of) the free energy available in the system is radiated away at GHz frequencies by coherent charge “patches” via e.g. curvature or synchrotron processes. However, the properties of the emitting particles/plasma and conditions for coherent emission have not been discussed in detail and will be the focus of this paper.

[Cordes & Wasserman \(2016\)](#) used coherent curvature radiation to explain both FRBs and the MJy shot pulses from the Crab pulsar, but the formation and stability of the relativistic near neutral coherent patches³ in their model were not discussed. [Ghisellini \(2017\)](#) derived the general conditions for synchrotron maser emission; GHz synchrotron emission requires weak (and ordered) magnetic field ($\lesssim 10^3/\gamma^2 \text{ G}$ for electrons and $\lesssim 10^6/\gamma^2 \text{ G}$ for protons) which can be found at distances $\gtrsim 10^{8-9} \text{ cm}$ from a neutron star for a dipole field configuration $B \propto r^{-3}$; where γ is the Lorentz factor of particles perpendicular to the B-field. [Ghisellini \(2017\)](#) pointed out that the energy requirement for FRBs may be hard to satisfy for the synchrotron maser model if FRBs are at cosmological distances. In an earlier paper, [Lyubarsky \(2014\)](#) proposed that synchrotron maser emission may be produced when a magneto-

hydrodynamic wave generated in a magnetar giant flare interacts with the surrounding pulsar wind nebula at a distance of $\gtrsim 10^{16} \text{ cm}$ (here $B \propto r^{-1}$). The common problem of [Ghisellini \(2017\)](#) and [Lyubarsky \(2014\)](#) models is that they did not discuss how the particle distribution (population inversion) for efficient maser emission can be achieved.

Most FRBs models are based on neutron stars (NS), which could naturally explain their short durations, large energy requirement, ordered magnetic field (hereafter B-field) needed for coherent emission, and repetitions with intervals between $\sim 10^2$ to $\gtrsim 10^7$ seconds (the only repeater so far is FRB 121102, but others may also be repeating, see [Lu & Kumar 2016](#)). In this paper, we use general physical considerations to show that the B-field in the FRB source plasma should be $\gtrsim 10^{14} \text{ G}$ and hence FRBs are most likely to be produced in the magnetosphere of a NS or stellar-mass black hole. We also note that the persistent radio source near FRB 121102 is consistent with being a supernova remnant (SNR) energized by a young NS/magnetar ([Metzger et al. 2017](#); [Kashiyama & Murase 2017](#)), although the possibility of an active galactic nuclei (AGN) cannot be ruled out ([Tendulkar et al. 2017](#)).

Much of the work presented in this paper was done in the summer of 2016, but the writing up of the paper took a long time due to some pressing matter. We have made every effort to cite papers related to this work that have been published in the meantime in this fast developing field.

In §2, we provide estimates for the size of the source region, and the strength of the electric field associated with the FRB radiation at the source. In §3, we show that coherent curvature radiation in neutron star magnetosphere can explain the FRB properties, and we also provide a number of arguments to show that the B-field strength should be $\gtrsim 10^{14} \text{ G}$. Some predictions of this model are discussed in §4, and a summary of the main results are provided in §5.

2 GENERAL CONSIDERATIONS

We provide a broad-brush picture of the FRB source in this section based on general physics considerations.

Considering that the FRB radiation is coherent, the size of the source along the line of sight cannot be larger than the wavelength (λ) of the radiation we observe. If the source is moving toward us with a Lorentz factor γ , the frequency in the source frame is smaller than in the lab frame by a factor γ , and the transverse size corresponding to the wavelength is $\gamma\lambda$. Since particle velocities are $(1 - \gamma^{-2})c$, separation of λ along the line of sight can be maintained over a lab-frame time $\sim \gamma^2\lambda/c$. The transverse source size is often taken to be $\ell_t = \gamma\lambda$. However, this need not be the case. The transverse size can be larger than $\gamma\lambda$ by factor $\eta^{1/2}$ and still coherence can be maintained; $\eta \equiv (\ell_t/\gamma\lambda)^2$. This is because the time delay between the arrival of photons at the observer from the opposite ends of the source in the transverse direction $\eta(\gamma\lambda)^2/(c \min\{d_A, d_t\})$ is smaller than $\nu^{-1} = \lambda/c$ provided that $\eta < [\min\{d_A, d_t\}/(\gamma^2\lambda)]$; where d_A is the angular diameter distance to the source, and d_t is the distance between the source and the *trigger point* — located behind the source — from which the signal originates and propagates outward and triggers different points in the source to start radiating. For FRBs at distances $d_A \sim 10^{28} \text{ cm}$, the requirement on η is

$$\eta^{1/2} \lesssim \min\{d_{t,6}^{1/2}, 10^{11} d_{A,28}^{1/2}\} \nu_9^{1/2} \gamma_2^{-1}. \quad (3)$$

Moreover, the shape of the coherent patch in the transverse direc-

² It should be noted that [Tendulkar et al. \(2016\)](#) failed to observe a FRB during SGR1806-20’s big outburst.

³ To explain the MJy shot pulses from the Crab pulsar, the coherent patch has fractional charge (net charge divided by the total number of particles) $\lesssim 10^{-7}q$; particles of positive and negative charges are moving in the same direction. The basic reason for requiring an extremely small fractional charge is that the energy of FRB electromagnetic waves comes from particles’ initial kinetic energy in the model of [Cordes & Wasserman \(2016\)](#). The cooling time is much shorter than 1 ns (see §3) unless an amount of net charge q is associated with kinetic energy $\gg \gamma m_e c^2$. Another reason for quasi-neutrality is the electrostatic repulsion.

tion is unknown. In the following, we take the area of the coherent patch in the transverse direction to be

$$A_{coh} \equiv \eta\gamma^2\lambda^2, \quad (4)$$

where $\eta = \eta_x\eta_y$ contains two multiplication factors η_x and η_y corresponding to the directions of the two principal axes in the transverse plane.

Thus, the maximum coherent volume in the lab frame is

$$V_{coh} \sim \eta\gamma^2\lambda^3, \quad (5)$$

and in the comoving frame

$$V'_{coh} \sim \eta\gamma^3\lambda^3. \quad (6)$$

This coherent patch contributes to the FRB radiation for a time duration of order $\nu^{-1} = \lambda/c$ in the observer's frame, during which the source has traveled a distance $\sim \gamma^2\lambda$ (in the lab frame) toward the observer. The patch turns off after this time and another patch lights up so that the intrinsic FRB duration is much longer than ν^{-1} . There could be more than one coherent patches (N_{patch}) adding up incoherently, and a continuous plasma flow could produce coherent radiation for a duration longer than ν^{-1} ; two sources that are separated by a distance larger than the size of a coherent zone are treated as two independent patches, and even within a coherent zone we can have multiple patches if the radiation they produce is not in phase. If the same source produces coherent radiation continuously for a time duration longer than ν^{-1} (in observer's frame), then we tag it as a different source after time interval ν^{-1} and yet another source after $2\nu^{-1}$ and so on.

The total isotropic equivalent of energy release for FRBs is $E_{iso} \sim 10^{40}$ erg and the isotropic equivalent luminosity is $L_{iso} \sim 10^{43}$ erg s $^{-1}$ (for a cosmological distance of $\sim 10^{28}$ cm). In the far field (Fraunhofer diffraction) limit, the solid angle within which electromagnetic (EM) waves add up coherently is⁴

$$\Omega_F \sim \pi(\eta\gamma^2)^{-1}. \quad (7)$$

If there are N_{patch} distinct coherent patches, each of volume $\sim V_{coh}$, contributing to the total observed FRB flux at any given time, the beaming corrected total energy is

$$E_{f\tau b} \sim \frac{E_{iso}\Omega_F}{4\pi N_{patch}} \sim (3 \times 10^{35} \text{ erg}) E_{iso,40} N_{patch}^{-1} \eta^{-1} \gamma_2^{-2}. \quad (8)$$

The average lab-frame energy density in EM waves in the radiating plasma is

$$\epsilon_{EM} \sim \frac{L_{iso}(\Omega_F/4\pi)}{cN_{patch}(V_{coh}/\lambda)} \sim \frac{L_{iso}}{4cN_{patch}\eta^2\gamma^4\lambda^2}, \quad (9)$$

which is of order $10^{21} L_{iso,43} N_{patch}^{-1} \eta^{-2} \gamma_2^{-4} \nu_9^2$ erg cm $^{-3}$. Therefore, the electric and magnetic field strengths associated with this EM wave energy density are

$$E_{\perp EM} = B_{\perp EM} \sim (4\pi\epsilon_{EM})^{1/2} \sim (10^{11} \text{ esu}) \frac{L_{iso,43}^{1/2} \nu_9}{N_{patch}^{1/2} \eta \gamma_2^2}, \quad (10)$$

where the B-field strength is in Gauss. The electric field is very strong in the sense that $qE_{\perp EM}\lambda/(m_e c^2) \sim 10^8$. Thus, unless

⁴ For a coherent patch with rectangular shape in the transverse direction and area $A_{coh} = \eta_x\eta_y\gamma^2\lambda^2$, the beaming solid angle $\Omega_F \sim \gamma^{-2} \min(\eta_x^{-1}, 1) \times \min(\eta_y^{-1}, 1)$. Equation (7) is only correct in the limit $\eta_x > 1$ and $\eta_y > 1$. For smaller η 's, the energy density associated with electromagnetic waves is larger than our current, conservative, estimate, because more energy is produced in a smaller coherent volume.

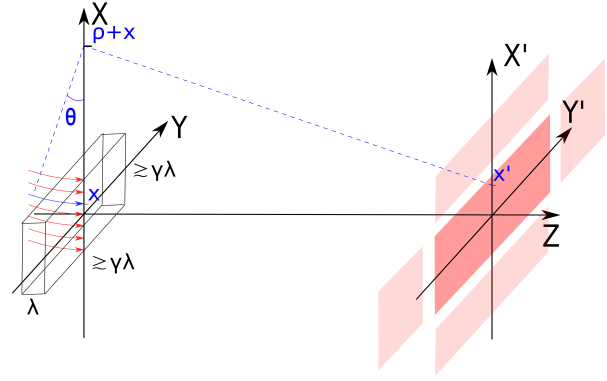


Figure 1. One slice of the plasma in the plane perpendicular to the line of sight. The distance between the source plane (X-Y) and image plane (X'-Y') is d . The coherent emitting volume has dimension $\Delta X \gtrsim \gamma\lambda$, $\Delta Y \gtrsim \gamma\lambda$ and $\Delta Z \sim \lambda$. The transverse area of the coherent patch is $A_{coh} = \eta\gamma^2\lambda^2$. In the far field (Fraunhofer diffraction) limit, the first fringe has area $\sim d^2(\eta\gamma^2)^{-1}$ and the observer is in this fringe.

this field is almost exactly perpendicular to the local magnetic field it will accelerate electrons to highly relativistic speeds and drain the energy out of the FRB radiation.

Since all the photons from a patch must be traveling in nearly the same direction and in phase in order that their fields add coherently, we therefore infer that the electric and magnetic fields associated with the observed FRB radiation calculated above is in a direction roughly perpendicular to the patch's velocity vector.

3 FRB SOURCE PROPERTIES: COHERENT CURVATURE RADIATION

Guided by general considerations of the last section that the B-field in the region where the observed radio photons from FRBs are produced is large, we restrict ourselves to the magnetosphere of a neutron star or a stellar-mass black hole. The curvature radiation — radiation produced when charged particles stream along curved B-field lines — is an efficient way in these conditions to produce large coherent radiation. In this section, we describe a detailed curvature radiation model that can reproduce observed FRB properties without any fine tuning of parameters.

Let us consider an electron moving with Lorentz factor γ along a B-field line of local curvature radius ρ . Due to its acceleration along the B-field curvature, the electron produces EM waves at frequency

$$\nu \approx \frac{c\gamma^3}{2\pi\rho}, \quad (11)$$

and the power radiated is

$$p_e \approx \frac{2q^2\gamma^4 c}{3\rho^2} \sim (2 \times 10^{-13} \text{ erg s}^{-1}) \nu_9^{4/3} \rho_5^{-2/3}. \quad (12)$$

The second expression for p_e is obtained by expressing γ in terms of ν using equation (11), i.e.

$$\gamma \approx 28 \nu_9^{1/3} \rho_5^{1/3}. \quad (13)$$

The electron's radiation is beamed in the forward direction within a cone of angle γ^{-1} , and the pulse time in the observer frame is smaller than the lab-frame time by a factor γ^2 . Thus, the isotropic

luminosity due to one electron, in the observer frame, is given by

$$\delta L_{iso} \approx \gamma^4 p_e \approx \frac{2q^2 \gamma^8 c}{3\rho^2} \sim (2 \times 10^{-7} \text{ erg s}^{-1}) \nu_9^{8/3} \rho_5^{2/3}. \quad (14)$$

Since we are considering radiation from a coherent patch where all electrons are moving with almost exactly the same velocity (γ) and streaming along nearly parallel B-field lines, we can take the patch to be moving with a Lorentz factor γ , and electrons in the patch's comoving frame to be essentially at rest. Let us consider that the electron density in the comoving frame is n'_e , which we express in terms of the Goldreich-Julian (GJ) density n_{GJ} (Goldreich & Julian 1969):

$$n'_e = \xi n_{GJ}, \quad \text{and in the lab frame } n_e = \gamma n'_e, \quad (15)$$

where

$$n_{GJ} \approx \frac{2B_0}{qcP} \left(\frac{R_{ns}}{R} \right)^3 \sim (10^{14} \text{ cm}^{-3}) P_{-1}^{-1} B_{0,14} \left(\frac{R_{ns}}{R} \right)^3. \quad (16)$$

R_{ns} , P and B_0 are the radius, rotation period and surface B-field strength of a neutron star, and R is the distance from the coherent patch to the center of the star. The spin down time for the neutron star due to dipole radiation is

$$t_{sd} \sim \frac{M_{ns} P^2 c^3}{\pi^2 B_0^2 R_{ns}^4} \sim (250 \text{ yr}) P_{-1}^2 B_{0,14}^{-2} R_{ns,6}^{-4}. \quad (17)$$

So if the object underlying FRBs is a neutron star with B-field strength $\sim 10^{14}$ G, then it can produce radio bursts for only a relatively short period of time of order a few hundred years. We note that the surface B-field B_0 of the FRB progenitor star may not be of dipole configuration; higher order multipole components give a smaller spin down power and hence a longer spin down time.

As our fiducial parameter, we take $\xi \sim 10$ and use $n'_e = 10^{15} n'_{e,15} \text{ cm}^{-3}$ hereafter, so the total number of electrons in the patch that are radiating coherently is

$$N_e = n'_e V_{coh} = \eta n'_e (\gamma \lambda)^3 \approx 6 \times 10^{23} \eta \nu_9^{-2} \rho_5 n'_{e,15}. \quad (18)$$

The isotropic equivalent luminosity, in the observer frame, due to N_{patch} coherent patches (each containing N_e electrons) can be calculated using equations (14) & (18)

$$L_{iso} = N_{patch} N_e^2 \delta L_{iso} \approx \frac{2c^7 q^2 \eta^2 \gamma^{14} (n'_e)^2 N_{patch}}{3\nu^6 \rho^2}, \quad (19)$$

or

$$L_{iso} \sim (10^{41} \text{ erg s}^{-1}) N_{patch} \eta^2 \nu_9^{-4/3} \rho_5^{8/3} (n'_{e,15})^2. \quad (20)$$

In arriving at the above equation we made use of equation (13). The observed FRB isotropic luminosity is $\sim 10^{43} \text{ erg s}^{-1}$, which can be easily accounted for if $\eta \sim 10$, $\rho_5 \sim 6$ or $n'_{e,15} \sim 10$ (or smaller values if some combination of these variables are adjusted). The beaming corrected luminosity in the lab frame is

$$L_{lab} \approx \frac{L_{iso} (\Omega_F / 4\pi)}{(\gamma^2 / 2)} \sim \frac{c^7 q^2 \eta \gamma^{10} (n'_e)^2 N_{patch}}{3\nu^6 \rho^2}, \quad (21)$$

$$L_{lab} \sim (4 \times 10^{34} \text{ erg s}^{-1}) N_{patch} \xi^2 \eta \nu_9^{-8/3} \rho_5^{4/3} (n'_{e,15})^2. \quad (22)$$

The factor in the numerator on the RHS of equation (21) is the solid angle of the radiation beam from the patch divided by 4π , and the factor in the denominator is the ratio of the observer frame and lab frame times.

The total kinetic energy of electrons in all radiating patches in the lab frame is

$$E_{ke} = \gamma m_e c^2 N_e N_{patch} \sim (1.5 \times 10^{19} \text{ erg}) \frac{\eta N_{patch} \rho_5^{4/3} n'_{e,15}}{\nu_9^{5/3}}. \quad (23)$$

Combining equations (22) & (23), we find the cooling time of electrons in the lab frame

$$t_{cool} \sim \frac{E_{ke}}{L_{lab}} \sim (3 \times 10^{-16} \text{ s}) \nu_9 (n'_{e,15})^{-1}, \quad (24)$$

which is much shorter (by a factor $\sim 10^9$) than the lab frame time duration ($\gamma^2 \nu^{-1}$) over which the patch is radiating. This requires that there is an electric field parallel to the B-field that can accelerate electrons and sustain their Lorentz factor at γ for the time duration of $\sim \gamma^2 \nu^{-1}$. The required electric field in the lab frame is given by

$$qE_{\parallel} \times ct_{cool} \sim \gamma m_e c^2 \text{ or } E_{\parallel} \sim (5 \times 10^9 \text{ esu}) \frac{\rho_5^{1/3} n'_{e,15}}{\nu_9^{2/3}}. \quad (25)$$

We can express the electric field in terms of the FRB luminosity using equation (20)

$$E_{\parallel} \sim (7 \times 10^{10} \text{ esu}) L_{iso,43}^{1/2} N_{patch}^{-1/2} \eta^{-1} \rho_5^{-1}. \quad (26)$$

This field, parallel to the B-field, is of the same order as the perpendicular electric field associated with the FRB radio emission (equation 10). The radiation can be sustained for a duration longer than ν^{-1} in the observer's frame provided that the electric field is maintained by some process for longer than $\gamma^2 \nu^{-1}$ (lab frame) such as an ongoing reconnection of B-field. In §3.2, we provide a possible magnetic reconnection geometry in which such a parallel electric field can be maintained.

The electric current associated with the motion of electrons in the volume V_{coh} is $I \sim q \gamma n'_e \eta (\lambda \gamma)^2 c$. The number density of particles with positive charge is nearly the same as the electron number density in order that the plasma is charge neutral. And since these positively charged particles are accelerated by the electric field in opposite direction to the electrons, the total current in the region is $2I$. Thus, the B-field generated by the current inside the patch is

$$B_{ind} \sim \frac{4\pi I}{c(\eta_x + \eta_y) \lambda \gamma} \sim 2\pi q \eta^{1/2} n'_e \lambda \gamma^2, \quad (27)$$

or

$$B_{ind} \sim (7 \times 10^{10} \text{ G}) \frac{\eta^{1/2} \rho_5^{2/3} n'_{e,15}}{\nu_9^{1/3}} \sim (10^{12} \text{ G}) \frac{L_{iso,43}^{1/2} \nu_9^{1/3}}{N_{patch}^{1/2} \eta^{1/2} \rho_5^{2/3}}. \quad (28)$$

This induced B-field is in the direction perpendicular to the primary B-field (\vec{B}_0), and the induced field lines are closed curves that lie in planes normal to \vec{B}_0 . Thus the superposition of the two fields $-\vec{B}_{ind}$ & \vec{B}_0 will point in different directions at different locations in the source. Particles are stuck in the lowest Landau state, as shown later, and therefore their motion is along B-field lines. In order for these particles to produce coherent radiation their velocity vectors should be nearly parallel. To be more precise, the angle between the velocity vectors for different particles should not be larger than γ^{-1} . This constraint provides a lower limit on the strength of the original B-field B_0 in the region:

$$B_0 \gtrsim \gamma B_{ind} \sim (5 \times 10^{13} \text{ G}) L_{iso,43}^{1/2} N_{patch}^{-1/2} \eta^{-1/2} \nu_9^{2/3} \rho_5^{-1/3}. \quad (29)$$

It is unphysical that a large number of patches would turn on *simultaneously* on a timescale of $\nu^{-1} \sim 1$ ns, so we expect that

$N_{patch} \sim 1$. Moreover, $\eta^{1/2}$ is at most of order unity, as been constrained in §2 (eq. 3). This means that FRBs are most likely produced near the surface of a neutron star or the event horizon of a stellar-mass black hole in a region where the B-field strength is $\gtrsim 10^{14}$ G.

3.1 Radio wave propagation through neutron star magnetosphere & constraint on particle density n_e

In this sub-section we discuss effects on GHz waves as they propagate through the magnetosphere of a neutron star. The main goal is to ascertain whether radio waves can propagate through this media without suffering excessive absorption, and to provide a constraint on the particle density in the region where FRB radiation is produced. We show below that wave absorption is small as long as the particle number density (n_e) is smaller than 10^{18} cm $^{-3}$, which is about 10^2 times the GJ density, i.e. $\xi \lesssim 10^2$ (note that $n'_e = \xi n_{GJ}$ and $n_e = \gamma n'_e$).

Transverse electromagnetic waves produced by the curvature radiation are linearly polarized with the electric field vector (\vec{E}_{EM}) perpendicular to both the local B-field (\vec{B}_0) and the wave-vector \vec{k} as long as $\omega_c \gg \omega_e$, where

$$\omega_e^2 = \frac{4\pi q^2 n'_e}{m_e} \quad \text{or} \quad \omega_e \approx (2 \times 10^{12} \text{ rad s}^{-1})(n'_{e,15})^{1/2}, \quad (30)$$

is the plasma frequency, and

$$\omega_c \equiv \frac{qB_0}{m_e c} = (1.8 \times 10^{21} \text{ rad s}^{-1})B_{0,14}, \quad (31)$$

is electron cyclotron frequency.

The condition for the propagation of transverse EM waves, with \vec{E}_{EM} perpendicular to \vec{B}_0 , in a highly magnetized plasma, is: $\omega > \omega_e^2/\omega_c$ (e.g. Arons & Barnard 1986). Therefore, although the plasma frequency in the FRB source region is much larger than FRB radio frequency, the GHz waves can still propagate through the medium at a speed that is extremely close to c .

It can be shown that as radio waves propagate through the magnetosphere with changing B-field direction, \vec{E}_{EM} adiabatically changes its direction so that it is perpendicular to both the local \vec{B}_0 & \vec{k} , as long as $\omega_e \gg \omega$ (see Cheng & Ruderman 1979).

In other words, the polarization vector of photons is along $\vec{k} \times \vec{B}_0$ while moving through the region of the magnetosphere where $\omega_e \gg \omega$.

The column density of electrons in the source region of FRB model we have described above is $\sim n'_e \gamma^3 \lambda \sim 10^{21} n_{e,15} \text{ cm}^{-2}$ (or 300 pc cm $^{-3}$). However, the contribution of the magnetosphere to the observed DM value of FRBs is negligible. This is due to the fact that the *effective plasma frequency* in the presence of a strong B-field is reduced by a factor of $(\omega_c/\omega)^{1/2} \sim 10^5$, and thus the contribution to the DM from the FRB source region is $\ll 1$ pc cm $^{-3}$.

3.1.1 Free-free absorption of GHz radiation

The FRB waves propagating through the medium where they are produced are subject to the free-free absorption process, which is calculated here. The standard result for free-free absorption (e.g. Rybicki & Lightman 1979) cannot be used for the FRB system because particle motion is restricted by the strong magnetic field and is essentially confined to one dimension. A self-consistent derivation of free-free opacity for the FRB source is presented below.

Consider Coulomb interaction between an electron (e^-) and a

proton (or positron) – hereafter p^+ – moving with Lorentz factors γ_e and γ_p , respectively. These particles are streaming along strong magnetic field lines of strength B_0 , and they remain in the lowest Landau state during the entire interaction. The angle between their momentum vectors is θ in the lab frame. We will use the method of virtual quanta to calculate Bremsstrahlung emission and absorption, which is carried out in the rest frame of the electron (prime frame), and then transformed back to the lab frame. The Lorentz factor of p^+ and the angle between the momentum vectors in the prime frame are given by

$$\gamma'_p = \gamma_p \gamma_e (1 + \beta_p \beta_e \cos \theta), \quad \beta'_p \gamma'_p \sin \theta' = \beta_p \gamma_p \sin \theta, \quad (32)$$

where $\beta'_p = v'_p/c$.

The x-axis is taken to be along the electron-momentum, and the x-y plane is the plane of e^- & p^+ momenta. The magnetic field in the prime frame at the location of the electron is

$$B'_x = B_0, \quad B'_y = B'_z = 0. \quad (33)$$

The main idea behind the virtual quanta technique is that the electromagnetic field due to p^+ in the prime frame is sharply peaked in a narrow region close to the particle. This field is Fourier decomposed and each frequency component is treated as a virtual photon that gets scattered by the electron.

The electric field components due to p^+ in the prime frame is calculated using the Liénard–Wiechert potential. We prefer to calculate the field in the p^+ rest frame and then Lorentz transform it to the prime frame followed by a rotation along the z-axis by an angle θ' so as to obtain field components along the x' and y' axes. The x' component of the electric field at the location of the electron is given by

$$E'_{x'} = -\frac{q\gamma'_p}{r_e'^3} [b' \sin \theta' + v'_p t' \cos \theta'], \quad (34)$$

where

$$r_e'^2 = b'^2 + \gamma_p'^2 v_p'^2 t'^2, \quad (35)$$

and b' is the minimum distance between e^- and p^+ in the prime frame.

For strong B_0 field associated with the FRB model, the y-component of the electric field and the magnetic field associated with p^+ are too weak and of too small a frequency to excite the electron to a higher Landau level and therefore these fields are ignored for the Bremsstrahlung calculation. The electron motion along the x' -axis is described by

$$\vec{\beta}'_e = -\frac{qE'_{x'}}{m_e c} \hat{x}'. \quad (36)$$

The electric field in the radiation zone due to the acceleration of the electron is

$$\vec{E}'_{rad} = \frac{q \hat{n}' \times [(\hat{n}' - \vec{\beta}'_e) \times \dot{\vec{\beta}}'_e]}{cr'(1 - \hat{n}' \cdot \vec{\beta}'_e)^3} \approx \frac{q}{cr'} [\hat{n}' \cos \psi' - \hat{x}'] |\dot{\vec{\beta}}'_e|, \quad (37)$$

where

$$\cos \psi' = \hat{n}' \cdot \hat{x}'. \quad (38)$$

The Poynting flux due to the electron acceleration is given by

$$\vec{S}' = \frac{c}{4\pi} \vec{E}'_{rad} \times \vec{B}'_{rad} = \frac{|\vec{E}'_{rad}|^2 c \hat{n}'}{4\pi}. \quad (39)$$

The energy release per unit frequency and per unit solid angle in a

$e^- - p^+$ scattering is

$$\frac{d\epsilon'}{d\omega' d\Omega'} = \frac{q^2 \sin^2 \psi'}{2\pi c} |\dot{\beta}'_e(\omega')|^2, \quad (40)$$

where

$$\dot{\beta}'_e(\omega') = \frac{q^2 \gamma'_p \hat{x}'}{(2\pi)^{1/2} m_e c} \int_{-\infty}^{\infty} dt' e^{i\omega' t'} \frac{(b' \sin \theta' + v'_p t' \cos \theta')}{(b'^2 + \gamma'^2_p v'^2_p t'^2)^{3/2}}. \quad (41)$$

This integral can be carried out using the modified Bessel functions

$$K_1(a) = \frac{a}{2} \int_{-\infty}^{\infty} dz \frac{e^{iz}}{(a^2 + z^2)^{3/2}}, \quad (42)$$

$$K_0(a) = \frac{1}{2i} \int_{-\infty}^{\infty} dz \frac{ze^{iz}}{(a^2 + z^2)^{3/2}}, \quad (43)$$

and we obtain

$$\dot{\beta}'_e(\omega') = \frac{2q^2 \omega'}{(2\pi)^{1/2} m_e c^3 (\beta'_p \gamma'_p)^2} \left[\gamma'_p \sin \theta' K_1 \left(\frac{b' \omega'}{v'_p \gamma'_p} \right) + i \cos \theta' K_0 \left(\frac{b' \omega'}{v'_p \gamma'_p} \right) \right], \quad (44)$$

where

$$\omega' = \omega \gamma_e (1 - \beta_e \cos \psi) \equiv \mathcal{D}^{-1} \omega, \quad \sin \psi' = \mathcal{D} \sin \psi. \quad (45)$$

Making use of equations (39) & (44), we obtain the energy release per unit frequency and per solid angle in one $e^- - p^+$ encounter

$$\frac{d^2 \epsilon}{d\omega d\Omega} = \mathcal{D}^2 \frac{d^2 \epsilon'}{d\omega' d\Omega'}, \quad (46)$$

or

$$\frac{d^2 \epsilon}{d\omega d\Omega} = \frac{q^6 \omega^2 \sin^2 \psi \mathcal{D}^2}{\pi^2 m_e^2 c^3 (v'_p \gamma'_p)^4} \times \left[\gamma'^2_p \sin^2 \theta' K_1^2 \left(\frac{b' \omega'}{v'_p \gamma'_p} \right) + \cos^2 \theta' K_0^2 \left(\frac{b' \omega'}{v'_p \gamma'_p} \right) \right]. \quad (47)$$

For a plasma with e^- and p^+ densities of n_e & n_p the Bremsstrahlung emissivity is given by

$$j^{ff}(\omega, \Omega) = n_e n_p 2\pi \int db b v_p \frac{d^2 \epsilon}{d\omega d\Omega}. \quad (48)$$

The emission is beamed along the electron momentum vector within an angle of γ_e^{-1} , and the spectrum peaks at $\omega \sim \gamma_e \gamma'_p (c/b') \sim \gamma_p \gamma_e^2 c n_e^{1/3}$ which is a factor $\sim 10^{10}$ larger than the GHz frequency of FRBs we are interested in. Therefore, we will consider the low frequency limit where

$$K_0(a) \approx -(\ln[a/2] + \xi'), \quad K_1(a) \approx 1/a, \quad (49)$$

$\xi' = 0.5772$ is the Euler-Mascheroni constant. It can be shown that for FRBs, the term containing K_0 in the above expression for j^{ff} is much smaller than the K_1 term. With these approximations, we finally arrive at the following simplified expression for Bremsstrahlung emissivity

$$j^{ff}(\omega, \Omega) \approx \frac{8q^6 n_e n_p \sin^2 \theta}{\pi m_e^2 c^4} \frac{(\gamma_e \psi)^2}{[1 + (\gamma_e \psi)^2]^4} \ln \left[\frac{b_{max}}{b_{min}} \right], \quad (50)$$

where ψ is the angle between electron momentum vector and the photon, and θ is the angle between e^- & p^+ momentum vectors; $b_{max}/b_{min} \sim m_e c^2 \gamma_e^3 / (\omega \hbar)$. The emissivity decreases very rapidly with angle for $\psi > \gamma_e^{-1}$.

Finally, we can obtain the expression for free-free absorption coefficient, including correction for the stimulated emission, in Rayleigh-Jeans limit using the Kirchhoffs law:

$$\kappa^{ff}(\nu, \psi) = j^{ff} / B_\nu(T) \approx \frac{\pi j^{ff} c^2}{k_B T \nu^2}, \quad (51)$$

or

$$\kappa^{ff}(\nu, \psi) \sim (5 \times 10^{-15} \text{ cgs units}) \frac{(\gamma_e \theta)^2 (\gamma_e \psi)^2 n_e^2}{\gamma_e^3 \nu^2 [1 + (\gamma_e \psi)^2]^4}, \quad (52)$$

where the electron temperature $k_B T \sim m_e c^2 \gamma_e$ along the magnetic field.

Inside the source region where the photons are moving almost parallel to electrons that produced them — $\psi \gamma_e \sim 1 \sim \theta \gamma_e$ — the optical depth corresponding to the source length ℓ along the line of sight is

$$\tau^{ff} \approx \kappa^{ff} \ell / (2\gamma_e^2) \sim 10^{-2} \ell_5 n_{e,17}^2 \nu_9^{-2}, \quad (53)$$

where we took $\gamma_e \sim 30$ as per equation (13). The optical depth due to particles moving in the direction opposite to the electrons is much smaller than that given by equation (53) for a electron-positron plasma⁵. For a electron-proton plasma, the absorption of GHz photons by protons is even smaller and can be ignored.

Equation (53) suggests that the particle density within the FRB source region should not be much larger than $\sim 10^{18} \text{ cm}^{-3}$ to avoid free-free absorption of photons. However, the allowed density is sufficient for producing the observed typical FRB luminosity of $L_{iso} \sim 10^{43} \text{ erg s}^{-1}$ for a coherent source of transverse size $\sim \gamma \lambda$, i.e. $\eta \sim 1$ (see eq. 20).

Once particles leave the acceleration zone the waves might suffer significant absorption if the outside temperature is much lower than $m_e c^2 \gamma_e / k_B$. This is, however, unlikely. The cooling time for electrons increases dramatically outside the *coherence zone*, and becomes of order $m_e c^2 \gamma_e / p_e \sim (10^8 \text{ s}) \nu_9^{-1} \rho_5$ (where p_e is taken from equation 12). In this case, the electron temperature stays relativistic and the free-free absorption at \sim GHz is small as long as the *coherence zone* is contained inside a somewhat larger acceleration zone. Moreover, as photons travel further out in the magnetosphere, the angle between their momentum vector and the local magnetic field direction (ψ) increases, and κ^{ff} decreases rapidly for $\psi \gtrsim \gamma_e^{-1}$ (as ψ^{-6} – see eq. 52) which keeps the free-free absorption small.

The free-free absorption increases with decreasing frequency as ν^{-2} , and therefore waves with $\nu \lesssim 500 \text{ MHz}$ are likely to be absorbed in the source region. This might explain the lack of detection of FRBs below GHz frequencies in a few cases.

The bottom line is that the GHz photons can escape the magnetosphere of a magnetar without suffering much free-free absorption provided that the plasma density in the source region $n_e \lesssim 10^{18} \text{ cm}^{-3}$. This upper limit to the density is larger than the GJ density by a factor $\sim 10^2$. Moreover, the density required for our model to produce the observed luminosity of a typical FRB of $L_{iso} \sim 10^{43} \text{ erg s}^{-1}$ is $n_e \sim 10^{17} \text{ cm}^{-3}$, and the transverse size of the source is

⁵ This is due to the fact that free-free radiation produced by positrons is narrowly beamed along their momentum vector, and very little radiation comes out in the opposite direction. Absorption of photons moving head-on toward positrons, which is related to the inverse of the free-free emission, has therefore, much smaller cross-section than absorption of photons moving in the same direction as positrons. The lower cross-section more than compensates for the larger number of positrons encountered by photons while traveling the distance w .

$l_t \sim \gamma\lambda$. The contribution to the DM of a FRB from the magnetar source region is negligible due to the modification of the EM wave dispersion relation in a highly magnetized plasma ($\omega_e/\omega_c \ll 1$).

3.2 Energy dissipation in current sheet to power FRBs

What we have established thus far, using general arguments, is that the B-field in the region where FRB GHz radiation is produced is $\gtrsim 10^{14}$ G, and the electric field component parallel to the B-field is $E_{\parallel} \sim 10^{11}$ esu. This electric field needs to be sustained for at least $1 \mu\text{s}$ ($\gamma^2\nu^{-1}$). In this sub-section we consider one possible way that such an electric field could arise: when inclined B-field lines in the magnetosphere of a neutron star are forced to come together and reconfigure. In this process of magnetic reconnection, a fraction of the B-field energy is dissipated and charged particles are accelerated by E_{\parallel} to relativistic speeds and produce coherent curvature radiation.

The calculations presented in this sub-section are less robust than other parts of the paper because the physics of reconnection and particle acceleration are poorly understood especially when the magnetization $\sigma = B_0^2/(4\pi n_p' m_p c^2)$ is large ($\sigma \gtrsim 10^{15}$ in the FRB source region). Fortunately, the uncertainties associated with the calculation of reconnection and E_{\parallel} do not affect other parts of this paper apart from some of the predictions of our model described in §4.

Let us consider the B-field directions at the opposite sides of the current sheet to be inclined at an angle $2\theta_B$, and B-field strength to be B_0 ; we consider $\theta_B \ll 1$ rad. The B-fields on the two sides of the sheet can be decomposed as parallel and anti-parallel components (see Fig. 2). Only the anti-parallel components of the B-field, which have strengths of $B_0 \sin \theta_B$, are dissipated inside the current sheet, whereas the parallel components with strength $B_0 \cos \theta_B$ (or the guide field) remain intact. Let us take the plasma speed flowing into the current sheet to be $\beta_{\text{in}}c$. The dimension of the current sheet along the line of sight (or along the guide field) is $\gtrsim \rho/\gamma$ and in the transverse direction is $l_x \gtrsim \eta^{1/2}\gamma\lambda$. The thickness of the current sheet is $l_y \gtrsim \eta^{1/2}\gamma\lambda$. Thus, the transverse area of the coherent volume is $A_{\text{coh}} = \eta\gamma^2\lambda^2$.

The dissipation rate of magnetic energy is

$$P_{\text{cs}} \simeq \frac{(B_0 \sin \theta_B)^2 \rho}{4\pi} \frac{1}{\gamma} \eta^{1/2} \gamma \lambda \beta_{\text{in}} c = \frac{E_{\parallel}^2}{4\pi \beta_{\text{in}}} \eta \rho \lambda c. \quad (54)$$

From the cooling time argument, we require $E_{\parallel} \simeq (L_{\text{iso}}/c)^{1/2} \eta^{-1} \rho^{-1}$ and hence

$$P_{\text{cs}} \simeq \frac{L_{\text{iso}}}{4\pi \beta_{\text{in}}} \frac{\eta^{1/2} \gamma \lambda}{\eta^2 \gamma \rho} \simeq \frac{L_{\text{lab}} \gamma}{\beta_{\text{in}} \eta^{1/2}} \quad (55)$$

where we have used $L_{\text{lab}} = L_{\text{iso}}/(2\eta\gamma^4)$ and $\lambda = 2\pi\rho/\gamma^3$. The radiation efficiency is

$$f_r \simeq \frac{L_{\text{lab}}}{P_{\text{cs}}} \simeq \frac{\beta_{\text{in}} \eta^{1/2}}{\gamma}. \quad (56)$$

The inflow velocity is also given by $E_{\parallel} = B_0 \sin \theta_B \beta_{\text{in}} \simeq (L_{\text{iso}}/c)^{1/2} \eta^{-1} \rho^{-1}$, i.e.

$$\beta_{\text{in}} \sin \theta_B \simeq 2 \times 10^{-3} B_{0,14}^{-1} L_{\text{iso},43}^{1/2} \eta^{-1} \rho_5^{-1}. \quad (57)$$

The angle θ_B can be roughly estimated from the condition that $|\vec{\nabla} \times \vec{B}| < 4\pi J_{\text{max}}/c$; where $J_{\text{max}} \sim qn_e c$. Since $|\vec{\nabla} \times \vec{B}| \sim B_0 \sin \theta_B / l_x$, we find that $\theta_B \lesssim 4\pi q n_e l_x / B_0 \sim 10^{-2} n_{e,17} \eta^{1/2} B_{0,14}^{-1}$. The system becomes charge starved for larger angles, and that would trigger rapid dissipation of magnetic fields. For $\theta_B \sim 10^{-2}$, we have $\beta_{\text{in}} \sim 0.2$ and hence

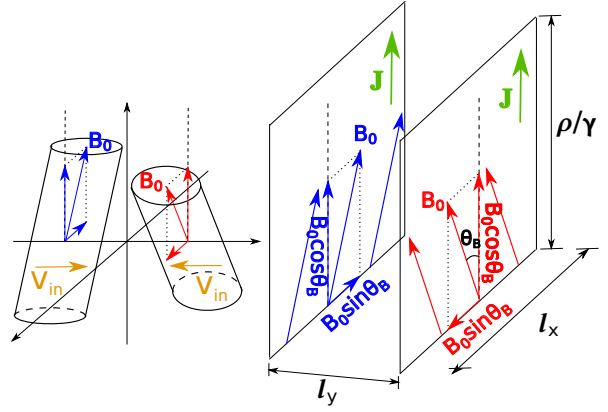


Figure 2. Geometry of the current sheet during magnetic reconnection. Plasma with inclined magnetic fields flow in at speed $v_{\text{in}} = \beta_{\text{in}}c$ from opposite sides into the current sheet. The electric field due to reconnection is $E_{\parallel} \sim B_0 \sin \theta_B \beta_{\text{in}}$ and is parallel to $B_0 \cos \theta_B$ (which is roughly parallel to the line of sight). The dimension of the current sheet along the line of sight is $\gtrsim \rho/\gamma$ and the transverse dimension is $l_x \gtrsim \eta^{1/2}\gamma\lambda$. The thickness of the current sheet is $l_y \gtrsim \eta^{1/2}\gamma\lambda$. In this way, the transverse area of the coherent volume is $A_{\text{coh}} = \eta\gamma^2\lambda^2$.

$f_r \simeq 7 \times 10^{-3} \eta^{1/2} \rho_5^{-1/3} \nu_9^{-1/3}$. There is considerable flexibility (and uncertainty) in values the parameters θ_B , B_0 , η and ρ can take, and hence a wide range of efficiencies from 10^{-4} to 10^{-1} are allowed in the magnetic reconnection model.

The intrinsic durations of most FRBs only have upper limits ~ 1 ms, because they were not resolved after deconvolution of the scattering broadening and DM smearing resulting from the finite channel width of radio telescopes. However, the repeating events from FRB 121102 showed various observed durations (2.8–8.7 ms) with no clear evidence of scattering broadening (Spitler et al. 2016). Also, FRB 121002 showed resolved double-peaked profile with separation of about 2.4 ms between the peaks (Champion et al. 2016). If we assume that these relatively long durations are intrinsic, the process that drives the magnetic reconnection may be relatively “slow”, i.e. operating on timescales much longer than the light-crossing time of the NS. The large scale steady state structure of the force-free NS magnetosphere (e.g. dipole or multipole with twists) can be solved (e.g. Akgün et al. 2016). However, the B-field configuration very close to the surface of a NS (most likely a magnetar for FRBs) is still poorly understood (e.g. Mereghetti 2008), so the mechanism for forced reconnection of magnetic fields is uncertain. One possible scenario is that magnetic flux emerges from below the NS surface due to buoyancy (e.g. Muslimov & Page 1995; Viganò & Pons 2012) and then the emergent B-field reconnects with pre-existing B-field in the magnetosphere at some inclination. Another possibility is the slow movement of the NS crust where the field lines are anchored. For example, in the first scenario, flux emergence from under the NS surface occurs on a timescale

$$t_{\text{em}} \sim \frac{H}{v_A} \sim (3 \text{ ms}) H_4 B_{0,14}^{-1} \rho_{0,14}^{1/2}, \quad (58)$$

where $H = 10^4 H_4$ cm is the depth from which the flux emerges, $\rho_0 = 10^{14} \rho_{0,14}$ g cm $^{-3}$ is mass density of the surface layer, $v_A = B_0/(4\pi\rho_0)^{1/2}$ is the Alfvén speed.

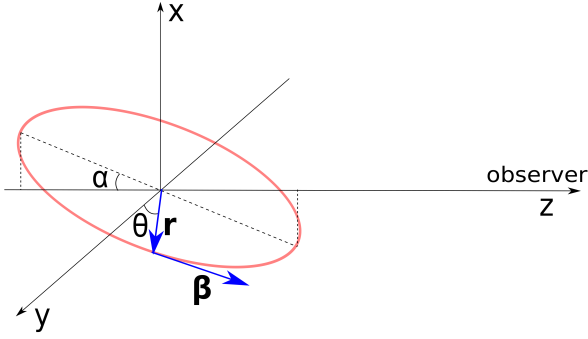


Figure 3. Geometry of a single radiating particle in a circular orbit with radius ρ . The observer is at $d \hat{z}$ on the z axis (line of sight), d being the distance. The orbital plane is tilted with respect to the z axis by an angle α . The position of the particle within the orbital plane is parametrized by the azimuthal angle θ , with $\theta = 0$ when the particle is on the y -axis. The position vector of the particle is \vec{r} and the velocity vector (divided by c) is $\vec{\beta}$. The retarded time $t_r = 0$ when the particle is on the x axis. The angular frequency is $\omega = \beta c/\rho$, so $\theta(t_r) = \omega t_r$.

3.3 Robustness of coherent curvature radiation

In §3.3.1, we calculate the radiation field from a single particle moving along a fixed B-field line, and then we add up the contribution from particles with different Lorentz factors and moving along magnetic field lines pointing in different directions. Taking $\rho = 10^5$ cm as an example, we show that the curvature radiation from different particles within a patch adds up coherently provided that (i) dispersion of the Lorentz factor of particles in the region is within a factor a few of the mean Lorentz factor (γ); (ii) the orientations of magnetic field lines at different points in the region are within an angle γ^{-1} of each other; (iii) the spectrum of the emergent coherent radiation can have strong fluctuations on \sim MHz scale; (iv) the time delay between radiation from opposite ends of the patch should be no larger than ν^{-1} .

In §3.3.2 & 3.3.3, we discuss a number of physical effects that could perturb particle trajectories, generate or inhibit the generation of coherent bunches.

3.3.1 Condition on particle velocity and B-field orientation distributions for coherent curvature radiation

Consider a single particle with charge q on a circular orbit of radius ρ (the curvature radius of the B-field line) inclined at an angle α with respect to the line of sight or \hat{z} axis, as shown in Fig. (3). The angular frequency is $\omega = \beta c/\rho$, where $\beta = |\vec{\beta}|$ is the particle's speed divided by c and we assume β to be constant with time in order to focus on the curvature radiation. The azimuthal angle at any retarded time t_r is given by $\theta(t_r) = \beta c t_r/\rho$ (we have taken $t_r = 0$ for $\theta = 0$). The electric field at the observer's location $d \hat{z}$ due to the particle's acceleration is (Rybicki & Lightman 1979)

$$\begin{aligned} \vec{E} &= \frac{q}{c\kappa^3 R} \vec{n} \times [(\vec{n} - \vec{\beta}) \times \dot{\vec{\beta}}], \\ &= \frac{q\beta\omega}{cd} \left[\frac{-\sin\theta \sin\alpha \hat{x} + (\cos\theta - \beta \cos\alpha) \hat{y}}{(1 - \beta \cos\theta \cos\alpha)^3} \right] \end{aligned} \quad (59)$$

where we have used $\kappa \equiv 1 - \vec{n} \cdot \vec{\beta}$, $\vec{n} \equiv \vec{R}/R$, \vec{R} being the vector from the particle's position to the observer, and we have neglected high order terms $O(\rho/d)$.

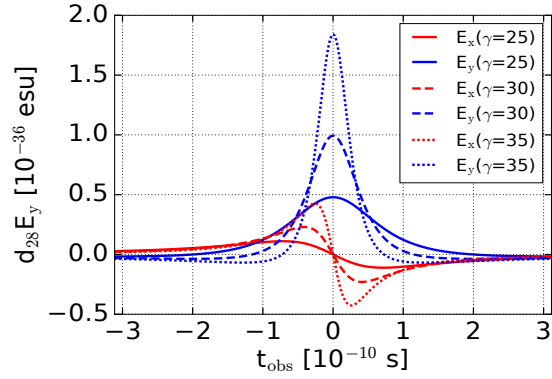


Figure 4. The electric field from a single electron at a distance of $10^{28} d_{28}$ cm according to equation (59). We consider three different Lorentz factors $\gamma = 25$ (solid lines), 30 (dashed lines), 35 (dotted lines); red lines are for E_x and blue lines are for E_y (see Fig. 3 for the definition of x and y axes). The curvature radius is $\rho = 10^5$ cm and the angle between the orbital plane and the line of sight is $\alpha = 0.5\gamma^{-1}$ radian. If there are N_e electrons on an identical trajectory, the total electric field is $N_e E$ and the isotropic luminosity is $L_{\text{iso}} = d^2 N_e^2 E^2 c$. For $N_e = 10^{24}$, $E = 10^{-36}$ esu at $d = 10^{28}$ cm means $L_{\text{iso}} = 3 \times 10^{42}$ erg s^{-1} .

We show in Fig. (4) the x and y components of the electric field in the far field due to a single particle. Note that E_x is anti-symmetric with θ and α while E_y is symmetric. If the particle flow is continuous on a timescale of $\gtrsim \nu^{-1}$, E_x from particles with positive and negative θ will cancel out, but E_y will survive. In the following, we only consider the \hat{y} component of \vec{E} , the magnitude of which is

$$\begin{aligned} E_y(t_{\text{obs}}) &= \frac{q\beta\omega}{cd} \left[\frac{\cos\theta(t_r) - \beta \cos\alpha}{(1 - \beta \cos\theta(t_r) \cos\alpha)^3} \right] \\ &\simeq \frac{q\gamma^4}{pd}, \text{ if both } \alpha \text{ and } \theta \ll \gamma^{-1}, \end{aligned} \quad (60)$$

where time t_{obs} in the observer frame is given by

$$t_{\text{obs}} = \int_0^{t_r} (1 - \vec{n} \cdot \vec{\beta}) dt_r \approx \int_0^{t_r} (1 - \beta \cos\alpha \cos\theta) dt_r. \quad (61)$$

The emission is strong only when $\alpha\gamma \lesssim 1$ and the duration of the emission from a single particle is $\Delta t_{\text{obs}} \sim \rho/(\gamma^3 c)$.

In Fig. (5), we plot the E_y from a coherent volume of electrons with flat distributions of Lorentz factors in the interval $20 < \gamma < 40$, orbital angles between $-\Delta\alpha < \alpha < \Delta\alpha$, and azimuthal angle in the interval $-\Delta\theta < \theta < \Delta\theta$. We consider three different $\Delta\alpha$ of $0.3/\gamma$, $1.0/\gamma$ and $3.0/\gamma$ radian; and three different $\Delta\theta$ of $0.3/\gamma^3$, $1.0/\gamma^3$, and $3.0/\gamma^3$; where $\gamma = 30$ is the mean Lorentz factor. The electric field is normalized to $N_e = 1$. To get the actual electric field, one needs to multiply with the total number of electrons in the coherent patch. The general conclusion is that coherence is destroyed and the resulting electric field E_y is much weaker when the separation of particles in a patch significantly exceeds λ (i.e. $\Delta\theta \gg \gamma^{-3}$) or when the direction of particle motion has a spread much larger than $1/\gamma$ (i.e. $\Delta\alpha \gg \gamma^{-1}$). Particle clumps with longitudinal size $\sim \lambda$ may be produced in various plasma instabilities, such as the two-stream instability (see §3.3.2).

We note that coherence at frequencies ~ 1 GHz is unaffected if particles have a broad Lorentz factor distribution. The peak frequency of curvature radiation depends strongly on the particle Lorentz factor $\nu \propto \gamma^3$, so particles with Lorentz factors larger (or smaller) than 30 by a factor of more than 2 will radiate most of their

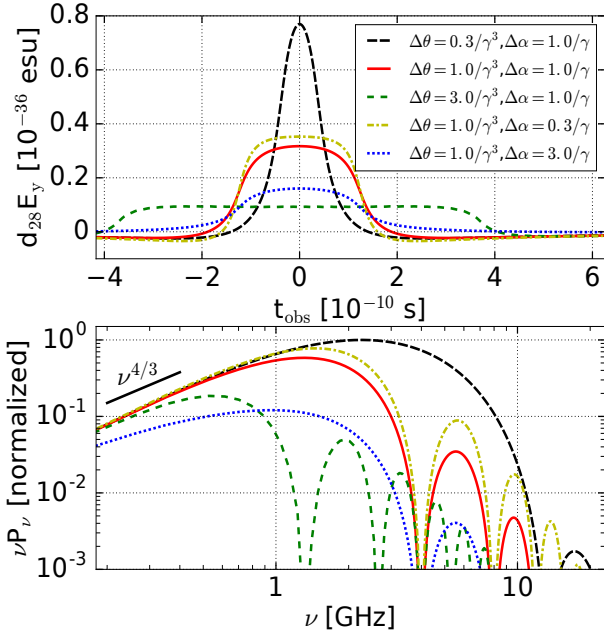


Figure 5. *Upper Panel:* The electric field from a bunch of electrons with flat Lorentz factor distribution $\partial N/\partial\gamma = \text{const}$ ($20 < \gamma < 40$), flat orbital plane angle distribution $\partial N/\partial\alpha = \text{const}$ ($-\Delta\alpha < \alpha < \Delta\alpha$), and flat azimuthal angle delay distribution $\partial N/\partial\theta = \text{const}$ ($-\Delta\theta < \theta < \Delta\theta$). The angle limits $\Delta\alpha$ and $\Delta\theta$ are expressed as functions of the mean Lorentz factor $\gamma = 30$ as shown in the legend. The total electric field is normalized to $N_e = 1$ (to get the actual electric field, one needs to multiply with the total number of electrons in the coherent patch). The source is at a distance of $10^{28} d_{28}$ cm. Since E_x is anti-symmetric with α and θ while E_y is symmetric, only E_y will contribute to observations. The pulse width increases with $\Delta\theta$. The shape is not strongly affected by $\Delta\alpha$, unless $\Delta \gtrsim 1/\gamma$ (when the peak electric field is much lower because the emission from a large fraction of electrons is beamed away from the observer). *Lower Panel:* The frequency spectrum normalized to the peak value of the ($\Delta\theta = 0.3/\gamma^3$, $\Delta\alpha = 1.0/\gamma$) case. The spectrum in the lower frequency end is $P_\nu \propto \nu^{4/3}$ and in the higher frequency end cuts off exponentially. For cases where $\Delta\theta \gtrsim 1.0/\gamma^3$, the pulse is like a step function; this is why the spectrum has regularly spaced discrete bumps (which resemble the discrete band structure seen in Crab pulses [Hankins & Eilek 2007](#)).

energy at frequencies much above (or below) ~ 1 GHz. During the reconnection, particles with a wide range of Lorentz factors may be produced, but that would not affect the observed luminosity of ~ 1 Jy at ~ 1 GHz provided that the number of particles with Lorentz factor ~ 30 (e.g. between 20 and 40) is of order 10^{24} . We also note that FRB spectrum depends on the Lorentz factor distribution $\partial N/\partial\gamma$. The radiation from particles with too large Lorentz factors will be beamed away from the observer line of sight, so we expect that there should be a sharp break in the FRB spectrum somewhere above 10 GHz (but not too far above 10 GHz, since the chance that an observer is within the beaming cone of particles with larger Lorentz factors decreases as γ^{-2}).

The observed FRB duration is affected by the DM smearing and broadening due to scatterings in the ISM/IGM. If the intrinsic duration of an FRB is δt_{in} (which is determined by the duration of magnetic reconnection), the number of coherent patches needed is $\sim \delta t_{\text{in}}/1 \text{ ns} \sim 10^6 \delta t_{\text{in}, -3}$; it should be pointed out that we receive radiation from only one of these patches at a time, and the million patches are part of a semi-continuous outflow in a current sheet which we have broken up into a large number of causally connected

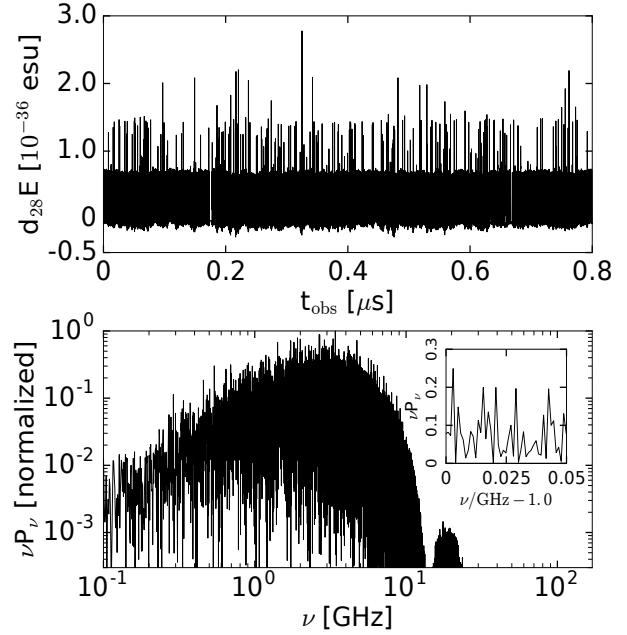


Figure 6. The emission from 2000 identical patches of the case with $\Delta\theta = 0.3/\gamma^3$ and $\Delta\alpha = 1.0/\gamma$ in Fig. (5). Adjacent patches are separated by δT , and δT is taken to be in Poisson distribution with mean value 5×10^{-10} s.

segments for the ease of calculation. As a simple demonstration, we show in Fig. (6) the emission from 2000 identical patches that turn on and off on a timescale of δT (in observer frame); δT is taken to have the Poisson distribution with mean value 5×10^{-10} s. The spectrum has strong fluctuations in frequency intervals as small as \sim MHz (Fig. 6). To model the observed FRB spectrum with rich fine-scale structure, one may need to add up contributions from different patches in more realistic ways. For example, particle flow could be episodic on μs –ms timescales and different patches could have different polarizations due to the rotation of the NS or non-stationary B-field configuration. Scintillation and plasma lensing probably also play an important role in shaping the observed spectrum (e.g. [Ravi et al. 2016](#)).

The EM emission directly coming from the source region is linearly polarized, with electric field perpendicular to the primary B-field and the line of sight. Due to the rotation of the NS, and the magnetic field orientation in the current sheet changing on μs timescale, the polarization angle is likely to be time dependent. The polarization state of photons can also change substantially as they propagate through plasma along the line of sight in the NS magnetosphere, magnetar wind nebula, and possibly supernova remnant. One would need to take these effects into consideration in order to model and interpret the polarization properties of FRB radiation.

3.3.2 Two stream instability in presence of electric field for relativistic relative velocity & its effect on coherent radiation

Since electrons and protons (or positrons) are accelerated by the nearly static electric field parallel to \vec{B}_0 in opposite directions, the two stream instability could have an effect on the coherent radiation generation. We show that this instability could lead to the formation of particle bunches with longitudinal size on the order of $\sim \lambda$ on timescales much shorter than $\gamma^2 \nu^{-1} \sim 1 \mu\text{s}$. We consider an electron-proton plasma, which is cold so that the state of the par-

ticles transverse to the B-field is in the lowest Landau level; the analysis here is applicable to electron-positron plasma as well.

Our choice of frame is such that protons are at rest in the absence of a wave, which simplifies the algebra, but does not restrict linear stability analysis. The notation in this subsection is different from the rest of the paper. We denote particle density in the fluid comoving frame without a prime (in previous sections we had used prime), and all remaining quantities are measured in the rest frame of the proton and are also denoted without a prime. Variables in the lab frame will be denoted by the subscript “lab”.

The electron and proton unperturbed densities in their comoving frames are n_e & n_p , and the perturbations are δn_e & δn_p respectively. The 4-velocities for electrons and protons (as measured in the comoving frame of unperturbed proton flow) are taken to be $u_e + \delta u_e$ and $u_p + \delta u_p$; $u_p = (1, 0, 0, 0)$. The perturbed equations for particle flux conservation follows from $(nu^\mu)_{,\mu} = 0$, and are

$$\delta n_{p,t} + n_p \delta u_{p,z}^z = 0 \quad (62)$$

$$n_e \delta u_{e,t}^t + \delta n_{e,t} u_e^t + (\delta n_e u_e^z + n_e \delta u_e^z)_{,z} = 0 \quad (63)$$

It follows from $u_p^\mu u_{p\mu} = -1$ and $u_p^z = 0$ (since perturbations are being carried out in the rest frame of protons) that $\delta u_p^t = 0$, but $\delta u_p^z \neq 0$. Moreover, perturbation of the equation $u_e^\mu u_{e\mu} = -1$, yields

$$u_e^t \delta u_e^t = u_e^z \delta u_e^z. \quad (64)$$

We use this relation to eliminate δu_e^t in equation (63)

$$\delta n_{e,t} + v \delta n_{e,z} + (n_e v / c \gamma) \delta u_{e,t}^z + (c n_e / \gamma) \delta u_{e,z}^z = 0, \quad (65)$$

where $\gamma \equiv u_e^t$, and $v/c \equiv u_e^z / u_e^t$.

The momentum equation for the cold plasma is: $T_{,\nu}^{\mu\nu} = q F^{\mu\nu} u_\nu - F_{rad}^\mu$ or $u^\nu u_{,\nu}^\mu = (q/m) F^{\mu\nu} u_\nu - F_{rad}^\mu / m$; where $T^{\mu\nu} = m n u^\mu u^\nu$ is the energy momentum tensor for cold plasma, $F^{\mu\nu}$ is the electro-magnetic second rank tensor, F_{rad}^μ is the radiation reaction force, and q and m are particle charge and mass. The z-component of the momentum equation is

$$u_{,t}^z + (u^z / u^t) u_{,z}^z = \frac{q}{m} E_z - \frac{F_{rad}^z}{m} \quad (66)$$

The electric field E_z is in the proton/positron comoving frame, but since particles are streaming in the z -direction, the z -component of electric field in the lab and electron comoving frames are also E_z . The electric force on a charged particle is balanced by the radiation reaction force, $qE_z - F_{rad}^z = 0$, for the unperturbed system. The perturbation to F_{rad}^z is a non-local quantity (because it depends on all the particles in the patch that are radiating coherently), and is not easy to include in the stability analysis of the system⁶. We ignore δF_{rad}^z in the perturbation analysis presented below, and due to this we might perhaps be overestimating the importance of the two-stream instability.

The perturbation of the z-component of the momentum equation for protons and electrons are:

$$\delta u_{p,t}^z = \frac{q}{m_p c} \delta E_z, \quad (67)$$

⁶ The effect of the radiation reaction force is likely to stabilize the system. An increase in qE_z , causes particles to be accelerated to a higher Lorentz factor, which then causes a higher radiative power output – curvature radiation power scales as γ^4 (equation 12) – and the resulting higher radiation reaction force tries to restore the equilibrium state of the system.

and

$$\delta u_{e,t}^z + v \delta u_{e,z}^z = -\frac{q \delta E_z}{m_e c}. \quad (68)$$

Finally, it follows from the Maxwell equations that

$$\delta E_{z,z} = 4\pi q [\delta n_p - \gamma \delta n_e - v n_e \delta u_e^z / c]. \quad (69)$$

Note that the density perturbation δn_e is defined in the electrons’ comoving frame, so we have the γ factor on the right-hand side because the equation is in the proton/positron rest frame.

Equations (62), (65), (67), (68) and (69) are five equations in five variables that we solve to determine the dispersion relation and two-stream instability growth time. Taking all perturbed variables to be proportional to $\exp(i\omega t - ikz)$, these five equations can be combined and reduced to the following two equations

$$-\frac{im_e c^2 \gamma (\omega - vk)^2}{v\omega - kc^2} \frac{\delta n_e}{n_e} + q \delta E_z = 0 \quad (70)$$

and

$$n_e \left[\frac{v(\omega - vk)}{v\omega - kc^2} - 1 \right] \frac{\delta n_e}{n_e} + ik \left[1 - \frac{\omega_p^2}{\omega^2} \right] \frac{\delta E_z}{4\pi q \gamma} = 0 \quad (71)$$

We finally obtain the dispersion relation, which is:

$$(\omega - vk)^2 \left[1 - \frac{\omega_p^2}{\omega^2} \right] - \frac{\omega_e^2}{\gamma^2} = 0, \quad (72)$$

where

$$\omega_p^2 \equiv \frac{4\pi q^2 n_p}{m_p}, \quad \text{and} \quad \omega_e^2 \equiv \frac{4\pi q^2 n_e}{m_e}. \quad (73)$$

The electron plasma frequency is

$$\omega_e \sim (2 \times 10^{12} \text{ rad s}^{-1}) n_{e,15}^{1/2} \quad (74)$$

It should be emphasized that k and ω are wavenumber and complex frequency in proton/positron rest frame; v and γ are the unperturbed velocity and Lorentz factor of the electron fluid in the rest frame of proton/positron, and n_e and n_p are particle number densities in the rest frame of electron and proton respectively.

It can be shown from equation (72) that two-stream instability is present when $[1 + (m_e \gamma^2 / m_p)^{1/3}]^{3/2} / (v \gamma k / \omega_e) < 1$, i.e. for sufficiently small wavenumber the system is unstable to bunching up of particles. The growth rate of instability, $\text{Im}(\omega)$, is obtained by finding the two complex roots of equation (72), which are complex conjugates of each other. The growth rate for $e^- - p^+$ and $e^- - e^+$ plasma for several different values of γ are shown in Fig. (7). Since γ in equation (72) is the electron Lorentz factor as measured in the rest frame of protons, it is equal to $2\gamma_{p,lab} \gamma_{e,lab}$, where $\gamma_{p,lab}$ and $\gamma_{e,lab}$ are Lorentz factors of protons and electrons measured in the lab frame.

Electron clumps of longitudinal size $\sim \lambda \sim 30$ cm are required for the coherent curvature radiation model considered in this work. The electron density needed to generate a typical FRB luminosity of $10^{43} \text{ erg s}^{-1}$ is $n_e \sim 10^{16} \text{ cm}^{-3}$ (see eq. 20 and the discussion following it — but note that n_e in this section is same as n'_e in that equation). Therefore, $\omega_e \sim 5 \times 10^{12} \text{ rad s}^{-1}$ (eq. 74). Hence, for a $e^- - p^+$ plasma of $\gamma_{e,lab} \sim 30$ (needed for the FRB curvature radiation, as per eq. 13), the clump size ($\sim 2\pi / k_{lab}$, for the fastest growing mode) turns out to be ~ 50 cm, and the growth time for the instability is about 30 ns in the lab frame (see Fig. 7); the time required for the formation of a clump is longer (due to causality limit), and is of order $0.5 \mu\text{s}$. For a $e^- - e^+$ plasma, clumps of size ~ 30 cm also form on a timescale of $\sim 0.5 \mu\text{s}$ in the lab frame. Since the emission from one coherent patch lasts for 1 ns in

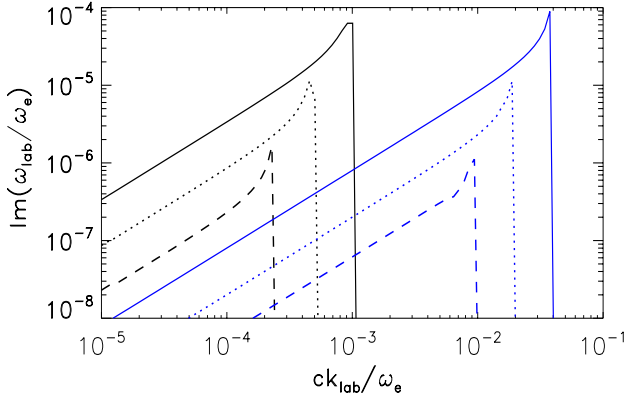


Figure 7. Shown here is the growth rate of two-stream instability in the lab frame — imaginary part of ω_{lab}/ω_e — for an electron-proton plasma with $\gamma_{e,lab} = \gamma_{p,lab} = 25, 50$ and 100 (black solid, dotted and dashed lines respectively) as a function of wavenumber in the lab frame; $\gamma_{e,lab}$ & $\gamma_{p,lab}$ are Lorentz factors of electrons and protons in the lab frame; we note that the Lorentz factor is independent of particle mass when acceleration is balanced by the radiation reaction. There are no unstable modes for the e-p plasma for $\gamma_{e,lab} = 25$ when $ck_{lab}/\omega_e \gtrsim 10^{-3}$. Also shown is the imaginary part of ω_{lab}/ω_e for electron-proton plasma with $\gamma_{e,lab} = \gamma_{p,lab} = 25, 50$ and 100 (blue solid, dotted and dashed lines respectively).

the observer frame, which corresponds to $\gamma_{e,lab}^2 \sim 10^3$ ns in the lab frame, particle clumps form on a time scale smaller than that required for the coherent curvature radiation to operate.

We note that the electric field associated with the clumping of electrons is much weaker than $E_{||}$ estimated in equation (26) and the electric field associated with the FRB EM wave energy $E_{\perp EM}$ in equation (10). Even in the extreme case where electrons are fully separated with protons/positrons in different clumps with longitudinal separation λ , the electric field due to clumping is roughly given by $E_{||,clump} \sim 4\pi N_e q / (\gamma_{e,lab}^2 \lambda^2)$, where N_e is the total number of particles in one clump and $\gamma_{e,lab}^2 \lambda^2$ is the transverse area of a coherent patch. For parameters required to produce FRB luminosities, $N_e \sim 10^{24}$, $\gamma_{e,lab} \sim 30$ and $\lambda \sim 30$ cm, we obtain $E_{||,clump} \sim 5 \times 10^9$ esu. In reality, the clumps are only partially charged and the electric field due to clumping is much smaller than this value. Therefore, the electric field associated with clumping will not be able to disperse the clumps; the back reaction of radiation on the clump can not disperse them either, because this reaction force is balanced by the reconnection electric field $E_{||}$ (eq. 26). Moreover, the electric field of charged clumps is not sufficiently strong to convert plasma waves to the EM waves at FRB luminosities.

3.3.3 Perturbation of particle trajectories by EM field and particle collisions — coherence survives

We showed in §3.3.1 that particle velocity distribution along the B-field need not be narrow for generation of coherent radiation. However, even a small dispersion in particle velocity perpendicular to the B-field can ruin the coherence. Also, the primary B-field lines along which particles in the source region are moving should be nearly parallel to each other (within an angle of γ^{-1}).

We show here that despite the presence of strong perpendicular electric and magnetic fields in the source region ($B_{ind} \sim 10^{12}$

G; equation 28), and collision between particles with opposite charges moving relative to each other at close to the speed of light, the distribution of particle velocity perpendicular to the B-field \vec{B}_0 is unaffected. The reason for this comes down to the fact that the energy of excited Landau levels are so large that particles stay in the ground state in spite of the large, time dependent, fields. And therefore, the coherence is preserved.

The energy of relativistic electrons in a magnetized medium is (see Appendix A)

$$\epsilon(p_z, n)^2 = m_e^2 c^4 + p_z^2 c^2 + 2\hbar\omega_c(n + 1/2)m_e c^2, \quad (75)$$

where p_z is the component of electron's momentum along the B-field line, n is a positive integer, and

$$\omega_c = \frac{qB_0}{m_e c} \quad (76)$$

is the electron cyclotron frequency. In the limit $p_z/(m_e c) \approx \gamma \gg 1$, the expression for electron energy can be approximated as

$$\epsilon(p_z, n) \approx p_z c + \hbar\omega_c(n + 1/2)/\gamma, \quad (77)$$

Thus, the energy of the electron corresponding to the lowest Landau level (for $n = 0$) is

$$\epsilon(p_z, 0) \approx p_z c + 1.1 \times 10^{-2} m_e c^2 B_{0,14}/\gamma_2 \quad (78)$$

The plasma temperature in the direction transverse to the B-field should be cold ($T \lesssim 10$ keV) — even though electrons are streaming along magnetic field lines with a Lorentz factor $\sim 10^2$ — otherwise higher Landau levels would be populated and the emergent radiation cannot be coherent.

The motion of electrons perpendicular to the B-field is damped due to the cyclotron radiation on a very short time scale of $\sim (10^{-17} \text{ s}) B_{0,14}^{-2} \gamma_2$ (in the lab frame). So the electron velocity dispersion perpendicular to the B-field (which is proportional to the transverse temperature) should be very small unless there is a mechanism or instability that operates on a much shorter timescale and excites electrons to higher Landau levels.

From equation (75) we see that the effective electron momentum transverse to the B-field, in the first excited level ($n = 1$), is $p_{\perp} = (3\hbar\omega_c m_e)^{1/2}$. This is much larger than the transverse momentum kick given to the electrons, $\sim q^2 n_e^{1/3}/c$ (classically), when electrons and protons undergo Coulomb collision in the FRB source. Particle collisions, therefore, cannot dislodge electrons from their ground Landau state.

The transverse electric field associated with FRB radiation is so strong ($E_{\perp EM} \sim 10^{11}$ esu; equation 10) that it shifts the energy of the Landau levels by an amount that is much larger than $\hbar\omega_c/\gamma$. However, it can be shown that this shift is exactly the same for all Landau levels, and since ω_c/γ is larger than the EM wave frequency (~ 1 GHz) by a factor $\sim 10^9$, electrons adapt to this periodic shift in the energy levels adiabatically and remain in the ground state, i.e. the strong EM field associated with the radiation does not kill the coherence.

The B-field produced by charged particles in the source region streaming along \vec{B}_0 is also strong ($B_{ind} \sim 10^{12}$ G; equation 28), and its direction changes on a length scale smaller than λ . However, electrons adapt to this changing B-field adiabatically since the de Broglie wavelength of electrons in transverse direction, $(2\hbar/\omega_c m_e)^{1/2} \sim 3 \times 10^{-9} B_{0,14}^{-1/2}$ cm (see Appendix A), is much smaller than the curvature radius of the B-field.

3.4 Propagation of radio waves through supernova remnant

Waves generated near the surface of a relatively young NS travel through the supernova remnant left behind in the explosion that produced the NS. We show in this sub-section that the contribution to DM from the supernova remnant is nearly constant for a period of a few years as required by the data for FRB 121102 from which 17 bursts have been detected (Spitler et al. 2016; Scholz et al. 2016); this point has already been made recently by (Murase et al. 2016; Piro 2016; Metzger et al. 2017). We also show that the optical depth of the supernova remnant for free-free absorption is small.

Let us consider that $10M_{\odot}$ of material is ejected in a supernova that produced the NS, and the initial speed of the remnant is 10^9 cm s⁻¹. The particle density of the medium in the vicinity of the explosion is taken to be 10 cm⁻³. In this case the deceleration radius for the remnant is $\sim 7 \times 10^{18}$ cm, and the deceleration time is about 200 years. The mean particle density of the ejecta t yrs after the explosion is $\sim 30t_2^{-3}$ cm⁻³, and the electron column density is $\lesssim 10^{20}t_2^{-2}$ cm⁻², if the ejecta is significantly ionized as suggested by Metzger et al. (2017); where $t_2 = t/(10^2$ yrs). Thus, the contribution of the ejecta to the FRB DM is $\sim 35t_2^{-2}$ pc cm⁻³. And the change to DM in three years is $\sim 2t_2^{-3}$ pc cm⁻³.

Seventeen radio bursts were detected from FRB 121102 in a period of 3 years, and the DM values for these events were the same (about 557 pc cm⁻³) during this period within the error of measurements. Thus, the age of the NS for this FRB cannot be smaller than 50 years. A similar lower limit on the age is obtained from the consideration that the DM from the host galaxy (at $z = 0.19$) does not exceed $\sim 10^2$ pc cm⁻³ (Tendulkar et al. 2017).

The free-free absorption optical depth for the remnant at 1 GHz is $\tau_{ff} \sim 3 \times 10^{-2}n_e^2t_2T^{-3/2} \sim 3 \times 10^{-5}t_2^{-5}T_4^{-3/2}$; where T is the temperature of the remnant. Tendulkar et al. (2017) find $\tau_{ff} \lesssim 10^{-3}$ for FRB 121102, and that too suggests the NS age to be $\gtrsim 50$ yrs.

It can be inferred from the large B-field strength of ($\gtrsim 10^{14}$ G) that the NS is most likely a magnetar. The empirical age of Galactic magnetars is $\sim 10^3$ to 10^4 yr (e.g. Viganò et al. 2013), which may be taken as the upper limit of the age of the FRB progenitor.

To summarize the main result of §3, the picture that emerges is that FRB radiation is produced in a patch of comoving size $\gamma\lambda$, where magnetic reconnection provides the necessary electric field to accelerate charged particles to Lorentz factor ~ 30 , and these particles produce coherent curvature radiation. The observed FRB radiation can be produced in a small region of transverse size $\sim 10^3$ cm (i.e. $\eta \sim 1$), with B-field strength of $\gtrsim 10^{14}$ G, and particle density of the order Goldreich-Julian density. The reconnection of the B-field is sustained for ~ 1 ms, and the electric field in the current sheet parallel to the primary B-field is $\sim 10^{11}$ esu.

4 PREDICTIONS OF THE MODEL

We provide in this sub-section a number of predictions of the model we have proposed for FRBs. In essence, the model is that radio waves are produced coherently in the magnetosphere of a NS with strong B-fields that undergo forced reconnection due to perhaps the movement of the neutron star crust (where the fields are anchored) or emergence of sub-surface flux tubes above the NS surface. The distortion of the B-field lines in the crust or magnetosphere builds up over a period of time, until it reaches a critical state and becomes

unstable and field lines are reconfigured, dissipating a fraction of the B-field energy in a current sheet in the process. This is a well known process and is responsible for the energy release in solar flares (e.g. Shibata & Magara 2011).

We begin by writing down the coherent curvature luminosity and the strength of the electric field parallel to the B-field in a nearly model independent form, and then specialize to magnetic reconnection to express length scales in terms of parameters appropriate for a current sheet.

$$L_{iso} \approx \frac{8\pi^2}{3} q^2 c (n'_e)^2 \ell_t^4 \gamma^4, \quad (79)$$

which is essentially the same as equation (19), except that we have taken $N_{patch} = 1$ (as discussed in §3), the transverse area of the source is ℓ_t^2 , and the expression for curvature radiation frequency (equation 11) has been used to eliminate the wavelength λ . The electric field strength (E_{\parallel}) is calculated by balancing the acceleration due to electric field with the radiation back reaction force (as was done in §3 leading to equation 25) and we re-express that result as:

$$E_{\parallel} \sim \frac{4\pi q n'_e \ell_t^2 \gamma^2}{3\rho} \sim \left[\frac{L_{iso}}{c\rho^2} \right]^{1/2}, \quad (80)$$

where as before ρ is the radius of curvature of the B-field.

Thus far we have not made any reference to reconnection and current sheets, and so the above results are broadly applicable. Next, we specialize to current sheets, and make a few predictions. Since we have a rather limited first-principle understanding of the properties of current sheets and particle acceleration, the following discussion is mostly qualitative.

The thickness of the current sheet is likely to be related to the plasma frequency (ω_p), and accordingly we take $\ell_t \sim \eta_p c / \omega_p$; where η_p is a dimensionless parameter which could be of order 10^2 – 10^3 as suggested by numerical simulations (e.g. Sironi et al. 2016). Substituting for ℓ_t in equation (80) we find

$$\gamma \sim \left(\frac{3qE_{\parallel}\rho}{\eta_p^2 m_e c^2} \right)^{1/2} \propto \eta_p^{-1} E_{\parallel}^{1/2} \rho^{1/2}, \quad (81)$$

which is independent of the plasma density (n'_e). Using equation (81) for γ , we calculate the frequency at which particles radiate most of their energy

$$\nu \sim \frac{\gamma^3 c}{2\pi\rho} \sim \frac{c}{2\pi\rho} \left[\frac{3qE_{\parallel}\rho}{\eta_p^2 m_e c^2} \right]^{3/2} \propto \eta_p^{-3} E_{\parallel}^{3/2} \rho^{1/2}, \quad (82)$$

and

$$L_{iso} \sim E_{\parallel}^2 \rho^2 c \propto \eta_p^4 \nu^4 \rho^{4/3}. \quad (83)$$

The electric field E_{\parallel} , B_0 , θ_B (the angle between field lines on the opposite sides of the current sheet), and η_p likely vary substantially from one reconnection event to another. Therefore, several general predictions can be made for FRBs according to the model described in this work.

(i) Electrons are likely accelerated to very different Lorentz factors in different bursts or different regions in one burst. Hence, in addition to the FRBs observed at a few GHz frequency, the model predicts that there are other FRBs that radiate at frequencies much higher than GHz (since $\nu \propto \gamma^3$); some FRBs may radiate most of the energy at 10 GHz whereas others might be at $\sim 10^{14}$ Hz. Since $\nu \propto E_{\parallel}^{3/2}$, it is unlikely to find FRBs at frequencies much larger than $\sim 10^{14}$ Hz; this is because $\nu \sim 10^{14}$ Hz requires

$E_{\parallel} \sim 10^{14}$ esu — which is of order the Schwinger limit on electric field strength of $m_e^2 c^3 / (q^2 \hbar)$ — and fields of larger strength cannot be sustained for long as they lead to spontaneous creation of electron-positron pairs and breakdown of the vacuum. High energy photons can be produced due to a process such as the resonant inverse-Compton scattering if the conditions in the source region are just right, but that requires fine tuning of parameters.

(ii) FRB event rate should decrease with increasing frequency roughly as⁷ $\gamma^{-2} \propto \nu^{-2/3}$, or perhaps more steeply, because of possible enhancement to the beaming associated with the transverse source size.

(iii) The intrinsic durations of FRBs at frequencies much larger than GHz may be of the same order as GHz-FRBs provided that there are a large number of independent beams (each of angular size γ^{-1}) that contribute to the total duration. On the other hand, if the radiation is produced by a single beam sweeping across the observer line of sight — which is the most conservative possibility for these transients — then the observed duration at higher frequencies would be smaller than a few ms since the higher frequency radiation is produced by electrons with larger Lorentz factors.

(iv) The luminosity function of FRBs in a fixed frequency band should be broad since $L_{\text{iso}} \propto \eta_p^4$. This might be the reason for the large flux variations (by at least an order of magnitude) observed for the different outbursts of the repeating FRB 121102 (Spitler et al. 2016; Scholz et al. 2016).

The intrinsic coherent radiation luminosity decreases with decreasing frequency, and the observed pulse width increases rapidly at lower frequencies due to wave scattering (roughly as ν^{-4} , but see Xu & Zhang 2016) by turbulence in the ISM/IGM and DM smearing (ν^{-3}). These effects cause the observed flux to decrease sharply at lower frequencies. To make matters worse, lower frequency waves may have difficulty in getting out of the supernova ejecta as a result of free-free absorption. So there is likely to be a low frequency cut-off to the FRB observations which might be of order a few hundred MHz.

5 SUMMARY & DISCUSSION

The very high brightness temperature of FRBs suggest that the radiation process is coherent, which means that the comoving source size cannot be larger than the comoving-frame wavelength λ' of the radiation we observe. Thus, the electric field associated with radiation at the source is of order 10^{11} esu (and the B-field is 10^{11} G). Furthermore we show that the curvature radiation can account for the observed FRB properties without any need for fine tuning. The current associated with charged particles' motion along field lines produces transverse B-field (with roughly cylindrical shaped field lines) that is sufficiently strong to perturb particle trajectories and destroy coherence unless the primary field is $\gtrsim 10^{14}$ G (see eq. 29). The strong B-field also ensures that electrons stay in the ground state of Landau levels in spite of several strong perturbations that are present in the source region that otherwise would excite particles to higher Landau level and destroy coherence. A particle density of $\sim 10^{17}$ cm⁻³ (in lab frame) is sufficient to account for the

⁷ One caveat is that the variation of FRB rate with frequency (for a given flux limit) depends on particles' Lorentz factor distribution $\partial N / \partial \gamma$, and the combined angular size of all the beams in case there are multiple beams associated with a source. The FRB rate $\propto \nu^{-2/3}$ should be taken as a rough estimate.

observed isotropic equivalent FRB luminosity 10^{43} erg s⁻¹; the total number of charged particles in one coherent patch with Lorentz factors $\gamma \sim 30$ is of order 10^{24} ; a coherent patch produces radiation for ~ 1 ns, and therefore the total number of particles responsible for a typical FRB transient is $\sim 10^{30}$, and the mass of this matter is about a kg for an electron-positron plasma.

However, because the particles are radiating in phase, their radiative cooling time is extremely small — of order 10^{-15} s or six orders of magnitude smaller than the wave period — unless there is a powerful acceleration mechanism that balances the radiative losses and maintains the particle speed. An electric field of strength $\sim 10^{11}$ esu, parallel to the primary B-field, is the required mechanism to sustain the particle motion for at least the lab-frame travel time ($\gamma^2 \nu^{-1} \sim \mu\text{s}$) over which GHz EM waves are produced. Such an electric field could be produced during forced magnetic reconnection near the surface of a magnetar. This could also explain why we see the bursts repeat episodically. The total energy release in these bursts, corrected for beaming, is estimated to be of order 10^{36} ergs, whereas the total energy in the B-field is at least $\sim 10^{45} B_{0,14}^2$ ergs.

The intrinsic durations of some FRBs may be much longer than the light-crossing time of a NS. If this is true, the process that drives the magnetic reconnection should be relatively “slow”. One possible scenario is that B-field flux emerges from below the NS surface due to buoyancy (e.g. Muslimov & Page 1995; Viganò & Pons 2012) and then reconnects with pre-existing B-field in the magnetosphere. Another possibility is the slow movement of the NS crust where the fields are anchored. It is currently unclear what this process might be.

According to the model we have described, the Lorentz factor of electrons (and hence the peak frequency of the spectrum), and the isotropic luminosity are dependent mainly on the thickness of the current sheet $\ell_t = \eta_p c / \omega_p$ (ω_p being the plasma frequency) and the strength of the electric field parallel to the B-field, E_{\parallel} . These two parameters could have large variations among different bursts or at different locations of one burst. Thus, according to the model we have described, the luminosity function for FRBs should be very broad. Also, the mechanism we have described should produce short duration bursts at frequencies much larger than 1 GHz⁸ (up to $\sim 10^{14}$ Hz). The rate of bursts, however, is predicted to decrease with increasing peak frequency because higher frequency photons require larger Lorentz factor of particles or smaller curvature radius of B-field. The former is a much stronger effect, and the burst rate is expected to decrease with frequency at least as $\nu^{-2/3}$.

There are several issues that we have not discussed in detail, which future works should address. In particular, studying the propagation of polarized waves through the NS magnetosphere and surrounding medium in the host galaxy may help our understanding of the odd spectrum of FRBs and their polarization properties. The distortion of B-field lines, and reconnection for an extremely large magnetization parameter plasma ($\sigma \gtrsim 10^{15}$) are also topics that require separate investigations.

6 ACKNOWLEDGMENTS

We thank M. Bailes, D. Lorimer, E. Petroff, M. Lyutikov, A. Spitkovsky, A. Piro, J. Cordes and A. Stebbins for discussions of

⁸ Waves at frequencies much smaller than 1 GHz may suffer from free-free absorption by the surrounding medium (e.g. supernova remnant) and much more severe scattering broadening.

FRB observations and possible emission mechanisms, B. Zhang for reading the manuscript and for his excellent comments, and F. Guo and S. Paban for useful discussions regarding magnetic reconnection and quantum effects in strong magnetic field respectively. We are highly indebted to the referee, Jonathan Katz, for his careful reading of the manuscript and for his numerous excellent comments and suggestions that substantially improved the paper and clarified a number of conceptual issues. WL was funded by the Named Continuing Fellowship at the University of Texas at Austin.

REFERENCES

- Akgün, T., Miralles, J. A., Pons, J. A., & Cerdá-Durán, P. 2016, *MNRAS*, 462, 1894
- Arons, J., & Barnard, J. J. 1986, *ApJ*, 302, 120
- Burke-Spolaor, S., & Bannister, K. W. 2014, *ApJ*, 792, 19
- Champion, D.-J., Petroff, E., Kramer, M., et al. 2016, *MNRAS*
- Chatterjee, S., Law, C. J., Wharton, R. S., et al. 2017, arXiv:1701.01098
- Cheng, A. F., & Ruderman, M. A. 1979, *ApJ*, 229, 348
- Cordes, J. M., & Wasserman, I. 2016, *MNRAS*, 457, 232
- Connor, L., Sievers, J., & Pen, U.-L. 2016, *MNRAS*, 458, L19
- Dai, Z. G., Wang, J. S., Wu, X. F., & Huang, Y. F. 2016, arXiv:1603.08207
- Falcke, H., & Rezzolla, L. 2014, *A&A*, 562, A137
- Geng, J. J., & Huang, Y. F. 2015, *ApJ*, 809, 24
- Ghisellini, G. 2017, *MNRAS*, 465, L30
- Goldreich, P., & Julian, W. H. 1969, *ApJ*, 157, 869
- Gu, W.-M., Dong, Y.-Z., Liu, T., Ma, R., & Wang, J. 2016, *ApJL*, 823, L28
- Hankins, T. H., & Eilek, J. A. 2007, *ApJ*, 670, 693
- Ho, W.C.G., Dong, L., Potekhin, A.Y., and Chabrier, G., 2003, *ApJ* 599, 1293
- Kashiyama, K., & Murase, K. 2017, arXiv:1701.04815
- Kashiyama, K., Ioka, K., & Mészáros, P. 2013, *ApJL*, 776, L39
- Katz, J. I. 2014, *Phys. Rev. D*, 89, 103009
- Katz, J. I. 2016, *Modern Physics Letters A*, 31, 1630013
- Katz, J. I. 2016, *ApJ*, 826, 226
- Katz, J. I. 2016, *ApJ*, 818, 19
- Katz, J. I. 2016, arXiv:1611.01243
- Katz, J. I. 2017, arXiv:1702.02161
- Keane, E. F., & Kramer, M. 2008, *MNRAS*, 391, 2009
- Keane, E. F., & Petroff, E. 2015, *MNRAS*, 447, 2852
- Kulkarni, S. R., Ofek, E. O., Neill, J. D., Zheng, Z., & Juric, M. 2014, *ApJ*, 797, 70
- Loeb, A., Shvartzvald, Y., & Maoz, D. 2014, *MNRAS*, 439, L46
- Lorimer, D. R., Bailes, M., McLaughlin, M. A., Narkevic, D. J., & Crawford, F. 2007, *Science*, 318, 777
- Lu, W., & Kumar, P. 2016, *MNRAS*, 461, L122
- Luan, J., & Goldreich, P. 2014, *ApJL*, 785, L26
- Lyutikov, M., Burzawa, L., & Popov, S. B. 2016, arXiv:1603.02891
- Lyubarsky, Y. 2014, *MNRAS*, 442, L9
- Marcote, B., Paragi, Z., Hessels, J. W. T., et al. 2017, *ApJL*, 834, L8
- Masui, K., Lin, H.-H., Sievers, J., et al. 2015, *Nature*, 528, 523
- Mereghetti, S. 2008, *A&ARv*, 15, 225
- Metzger, B. D., Berger, E., & Margalit, B. 2017, arXiv:1701.02370
- Mickaliger, M. B., McLaughlin, M. A., Lorimer, D. R., et al. 2012, *ApJ*, 760, 64
- Murase, K., Kashiyama, K., & Mészáros, P. 2016, *MNRAS*, 461, 1498
- Muslimov, A., & Page, D. 1995, *ApJL*, 440, L77
- Pen, U.-L., & Connor, L. 2015, *ApJ*, 807, 179
- Petroff, E., van Straten, W., Johnston, S., et al. 2014, *ApJL*, 789, L26
- Petroff, E., Johnston, S., Keane, E. F., et al. 2015, *MNRAS*, 454, 457
- Petroff, E., Bailes, M., Barr, E. D., et al. 2015, *MNRAS*, 447, 246
- Petroff, E., Barr, E. D., Jameson, A., et al. 2016, *PASA*, 33, e045
- Piro, A. L. 2012, *ApJ*, 755, 80
- Piro, A. L. 2016, *ApJL*, 824, L32
- Popov, S. B., & Postnov, K. A. 2010, *Evolution of Cosmic Objects through their Physical Activity*, 129
- Potekhin, A. Y., & Chabrier, G. 2003, *ApJ*, 585, 955
- Rane, A., Lorimer, D. R., Bates, S. D., et al. 2016, *MNRAS*, 455, 2207
- Ravi, V., Shannon, R. M., Bailes, M., et al. 2016, *Science*, 354, 1249
- Romero, G. E., del Valle, M. V., and Vieyro, F. L., 2016, *Phy Rev D*, 93, 3001
- Rybicki, G. B., & Lightman, A. P. 1979, *New York, Wiley-Interscience*, 1979. 393 p.
- Scholz, P., Spitler, L. G., Hessels, J. W. T., et al. 2016, *ApJ*, 833, 177
- Sironi, L., Giannios, D., & Petropoulou, M. 2016, *MNRAS*, 462, 48
- Shibata, K., & Magara, T. 2011, *Living Reviews in Solar Physics*, 8, 6
- Spitler, L. G., Scholz, P., Hessels, J. W. T., et al. 2016, *Nature*, 531, 202
- Tendulkar, S. P., Kaspi, V. M., & Patel, C. 2016, *ApJ*, 827, 59
- Tendulkar, S. P., Bassa, C. G., Cordes, J. M., et al. 2017, *ApJL*, 834, L7
- Totani, T. 2013, *PASJ*, 65,
- Thornton, D., Stappers, B., Bailes, M., et al. 2013, *Science*, 341, 53
- Viganò, D., & Pons, J. A. 2012, *MNRAS*, 425, 2487
- Viganò, D., Rea, N., Pons, J. A., et al. 2013, *MNRAS*, 434, 123
- Xu, S., & Zhang, B. 2016, *ApJ*, 832, 199
- Zhang, B. 2014, *ApJL*, 780, L21
- Zhang, B. 2017, arXiv:1701.04094

APPENDIX A: LANDAU LEVELS FOR RELATIVISTIC PARTICLES

We calculate the energy states of a charged particle in a strong B-field. Particle speed along the field line is highly relativistic, and the field is very strong so that the particle spin is aligned with the field. We, therefore, ignore particle spin, and consider Klein-Gordan equation with magnetic potential (the electric field is taken to be zero):

$$\left(i\hbar\vec{\nabla} - \frac{q\vec{A}}{c}\right)^2 \psi + m^2 c^2 \psi = -\frac{\hbar^2}{c^2} \frac{\partial^2 \psi}{\partial t^2}, \quad (\text{A1})$$

or

$$\hbar^2 \nabla^2 \psi + \frac{2i\hbar q}{c} \vec{A} \cdot \vec{\nabla} \psi + \frac{i\hbar q}{c} (\vec{\nabla} \cdot \vec{A}) \psi - \frac{q^2 A^2}{c^2} \psi - m^2 c^2 \psi = \frac{\hbar^2}{c^2} \frac{\partial^2 \psi}{\partial t^2}. \quad (\text{A2})$$

Let us consider a uniform B-field, $\vec{B} = B_0 \hat{z}$, and vector potential $\vec{A} = -yB_0 \hat{x}$ corresponding to it. The wave function has a non-trivial dependence on the y -coordinate, and we express it as

$$\psi(\vec{x}, t) = u(y) \exp(ip_z z/\hbar + ip_x x/\hbar - iEt/\hbar), \quad (\text{A3})$$

and substitute that in the Klein-Gordan equation to obtain

$$\frac{d^2 u}{dy_1^2} + \frac{u}{\hbar^2 c^2} [E_1^2 - q^2 B_0^2 y_1^2] = 0, \quad (\text{A4})$$

where

$$y_1 \equiv y - \frac{cp_x}{qB_0}, \quad \text{and} \quad E_1^2 \equiv E^2 - p_z^2 c^2 - m^2 c^4. \quad (\text{A5})$$

The equation for u is that of a harmonic oscillator, and therefore the quantum states have energies as follows:

$$E_1^2 = 2qB_0 c \hbar (n + 1/2), \quad (\text{A6})$$

or

$$E^2 = m^2 c^4 + p_z^2 c^2 + 2\hbar\omega_c (n + 1/2) m c^2, \quad (\text{A7})$$

where

$$\omega_c = \frac{qB_0}{mc} \quad (\text{A8})$$

is the cyclotron frequency.

The wave function u_n , for the Landau state n , is given by:

$$u_n(y_1) = \frac{1}{\sqrt{2^n n!}} \left[\frac{2m\omega_c}{\hbar} \right]^{1/4} e^{-\frac{m\omega_c y_1^2}{2\hbar}} H_n(y_1 \sqrt{m\omega_c/\hbar}), \quad (\text{A9})$$

where H_n is the Hermite polynomial of n -th order

$$H_n(x) = (-1)^n e^{x^2} \frac{d^n}{dx^n} e^{-x^2}. \quad (\text{A10})$$

The spatial extent of the wave-function in the ground state is

$$\lambda_{DB\perp} \sim \sqrt{\frac{2\hbar}{m_e \omega_c}} \quad (\text{A11})$$

This is a result that we use in §3.